Clemson University
TigerPrints

All Theses | Theses

5-2017

Trunk Robot for Extended Environments

Siddharth R. Verma
Clemson University, siddhav@g.clemson.edu

Follow this and additional works at: https://tigerprints.clemson.edu/all_theses

Recommended Citation
Verma, Siddharth R., "Trunk Robot for Extended Environments" (2017). *All Theses*. 2680.
https://tigerprints.clemson.edu/all_theses/2680

This Thesis is brought to you for free and open access by the Theses at TigerPrints. It has been accepted for inclusion in All Theses by an authorized administrator of TigerPrints. For more information, please contact kokeefe@clemson.edu.

TRUNK ROBOT FOR EXTENDED ENVIRONMENTS

A Thesis
Presented to
the Graduate School of
Clemson University

In Partial Fulfillment
of the Requirements for the Degree
Master of Science
Electrical Engineering

---

by
Siddharth R. Verma
May 2017

Accepted by:
Dr. Ian D. Walker, Committee Chair
Dr. Apoorva D. Kapadia
Dr. Adam W. Hoover

ABSTRACT

We describe the design and physical realization of a novel type of large-scale continuum robot. The design, based on a hybrid concentric-tube/tendon actuated structure, is realized at a significantly larger scale than previous concentric tube continuum robots, with an extended length well over one meter. While operation at this scale opens up new types of potential applications, realization at this scale presents interesting challenges. We detail and discuss the associated issues via the prototyping and testing of the physical system with the help of experiments.

DEDICATION

To my parents and my sister for their unconditional support.

To my advisors for their timely guidance and support throughout the process.

ACKNOWLEDGMENTS

I would first like to acknowledge all of the guidance, support, and patience shown by my advisor, Professor Dr. Ian D. Walker. He gave me the opportunity to work on this project right from the proposal stage and believed in my ability to bring it to fruition. Dr. Walker always provided me with unbiased guidance gladly and I truly believe that this would not have been possible without him.

I would like to thank Dr. Apoorva D. Kapdia for his guidance and support during the course of my research and for accepting to be my committee member.

I would also like to thank Professor Dr. Adam W. Hoover for accepting to be my committee member.

Furthermore, I would like to thank everyone in the lab for providing helping hands and advice when it was needed.

TABLE OF CONTENTS

Page

Table of Contents (Continued) Page

LIST OF TABLES

LIST OF FIGURES

List of Figures (Continued) Page

CHAPTER ONE: INTRODUCTION

1.1 Continuum Robotics and Long Continuum Robots

Continuum robots have continuous, smooth bodies with no discrete “elbows” or “corners”. They are often compared to, and inspired by, biological tongues, trunks and tentacles. Continuum robotics as a field is still in its infancy. The snake robots of the early 1980’s [1] represent some of the earliest examples of continuum robots. Beginning with these designs, continuum robots have found use in a variety of fields, such as medicine [2], exploration, agriculture [3], inspection of hazardous and difficult to access environments [4], and biomimetics [5] [6]. Their targeted applications differ from those of ‘conventional’ rigid link robots, mainly because their smooth continuous bodies can provide a maneuverability which rigid link robots often cannot. They possess a fundamentally different structure and rely on large-to (theoretically)-infinite degrees-of-freedom to achieve a high level of compliance.

Traditional rigid-link robots differ from continuum robots in various important aspects, chiefly arising from their physical design. In contrast to rigid-link robots, continuum robots have a ‘smoother’ and a more compliant backbone enabling them to take a wide variety of curved shapes. Continuum manipulators are most useful in applications where the dexterity of the manipulator is of a higher priority than accuracy. Given their inherently flexible nature, continuum manipulators are well suited for navigating through curved spaces, grasping irregular objects or negotiating *a priori* unknown structures [7].

One example of a continuum robot is the OctArm, a pneumatically-driven continuum robot comprising 3 serially connected sections. Each section is made up of 3 McKibben actuators connected along the vertices of a virtual triangle where the relative differences in the actuating pressures allow the sections to bend in any direction in 3-D space. One major disadvantage of this design was the lack of a viable payload due to the mode of actuation, especially when attempting to work against gravity [8].

Most continuum robots developed so far have been at a relatively small scale, typically significantly less than one meter in length. At these scales, gravitational loading is either not a factor or has been handled on a largely *ad hoc* basis. However, as the scale increases, the effects of gravitational loading and payload effects become issues of greater significance [5]. This issue generally arises with soft robots mainly because of their flexible bodies. With close to the payload capacity of the robot, the moment applied at the tip of the robot cause it to take a curved shape due to being unable to generate the required amount of lift.

Several longer continuum robots have been demonstrated. In [9] for example, a thin continuum "Tendril" robot of length over one meter is detailed, aimed at the exploration of complex areas that are not easily accessible. However, the proposed applications were in Space, where gravity is not a factor. Another relatively long design (over one meter) is the "snake-arm robots" of OC Robotics, which are used in inspection operations [10]. However, these robots have segmented backbones, are not used as manipulators, and lack truly continuum structures.

Designing robot structures without a rigid backbone structure is an unconventional process, especially at the meter or more scale where the required payload capacities are higher and beyond the capabilities of existing thin continuum robots. However, there is significant motivation to bring the adaptability of continuum robot structures to bear at the multi-meter scale, as this could open up new application areas for robotics, such as in food service, warehousing, and construction.

The only example of a truly large-scale continuum robot to date is the EMMA™ [4] manipulator which was a 52.5 foot (16 meter) hyper-redundant manipulator aimed at waste tank remediation. EMMA™ used a tower system which would lower the entire 5-stage arm into the area of access and had a motor drive to enable it to rotate along the tower axis. However, for horizontal orientation of the manipulator, gravity would still play an important factor in limiting the reach and payload capacity of the robot.

Gravitational loading causes problems with scalability of continuum manipulators. Given the degree of compliance large-scale continuum robots are required to have, there is a tradeoff between expanding the working envelope and increasing the load capacity of the robot. Physical properties of the materials used can be an integral factor in the feasibility of scaling up a robot design.

1.2 Overview of Thesis

In this thesis, we address the challenges in building a large-scale continuum robot at the meter or larger scale with a sufficiently acceptable payload for its size. Specifically, we introduce the first concentric tube robot at the scale of greater than a meter. The novel

design exploits the material properties of the robot to provide sufficient support for horizontal orientation. The goal was to realize a large-scale robot that would have the dexterity of a conventional continuum robot but with a longer reach and have a payload capacity higher than that of thinner continuum counterparts in order to suit a new/different class of applications.

The following chapter contains an in-depth description of the physical development of the prototype discussing the structural design, spacer design, and actuation mechanisms. Chapter 3 describes basic tests that were conducted to evaluate the capabilities of the robot such as bending limits and load capacities of individual sections. Experimental evaluation is detailed in Chapter 3 where the robot demonstrates the ability to perform remote inspection, and maintenance tasks for a simulated glovebox enclosure for hazardous environments.

CHAPTER TWO: PROTOTYPING

2.1. Design Concept

The design for the robot introduced in this thesis was in response to pre-specified size and weight requirements and constraints. Since EMMA™ [4], there have not been continuum robots of a similar size and scale. At 52.5 feet long, EMMA was the first and the only manipulator of its kind and scale. The aim of constructing the Trunk Robot for Extended Environments (TREE) was to build a robot of a considerably large scale relative to the current state of the art, in order to significantly improve the payload capacities of continuum style robots for a tip load of about 5 pounds, at a length of about 5-6 feet.

While the Tendril [11], had its advantages of being able to explore difficult to reach spaces and access much more confined areas, it was also significantly affected by gravitational loading and had a low load capacity. The overall design goal of this thesis was to build an extensible continuum-style robot with a minimal number of tendons while providing the same amount of dexterity as the Tendril. In consideration of the success of concentric tube continuum robots used in medical applications at a significantly smaller scale [2], it was decided to investigate a concentric tube design for the robot (Figure 2.1). As in the case of medical continuum robots, linear actuators would actuate the extension and the retraction of the tubes relative to each other. Two linear actuators would be mounted behind the base of the proximal section and each actuator be connected to its respective section. Extension of the robot would be achieved via the linear actuators translating the tip section inside the middle section tube and the middle section within the base section tube.

In order to minimize the number of motors needed for tendons, two tendons were elected to be used per section, which would be spaced 180 degrees apart around the section circumference, to achieve sectional bending with two motors pulling the tendons, per section. Relative rotation between the tubes would be achieved by providing a motor to directly actuate relative rotational motion of each independent section tube. With three sections and each section having two tendons, there would be a total of six motors needed to achieve independent bending of each section. The motors for rotational motion (rotating the tubes about their main backbone axes) would be mounted on the base of their respective sections in order to achieve independent rotational motion. This would result in each section bending in one plane (defined by the plane including both of its tendons) and with the help of rotational motors, rotation of that plane about its axial tangent in order to access the full 3D workspace via 2D bending of each section as shown in Figure 2.1.

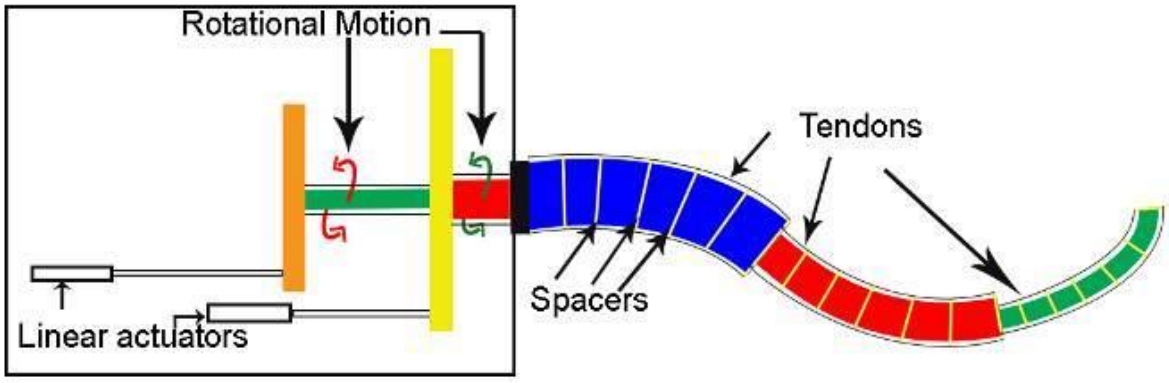

Figure 2.1 Blue: Proximal section, Red: Middle section, Green: Distal section

2.2. Structural Considerations for Backbone

In order to have the required flexibility as well as the necessary structural support, factors such as the length, diameter and material of the concentric tubes were crucial. It was observed that for effective bending of the tubes as well as smooth linear and rotational actuation, the three concentric sections would need to comprise of adequate complementary lengths for the proximal, middle and distal sections of the robot. It was determined that the desired robot functionality would be best achieved by these sections having lengths of 2’ (0.6m), 4’ (1.2m) and 6’ (1.8m) respectively, the schematic for which is shown in Figure 2.1. The initial design called for tubes of diameters ¼” (0.012m), 1 ¼” (0.04m) and 2” (0.05m) for the distal, middle and proximal sections respectively. With bending being based on tendons it was decided to use spacers for tendon routing, similar to EMMA [4]. With the tubes being concentric, the spacers needed to have very specific dimensions for smooth linear and rotational actuation. With this in mind, it was decided to make the spacers using an additive manufacturing, i.e. 3D, printer.

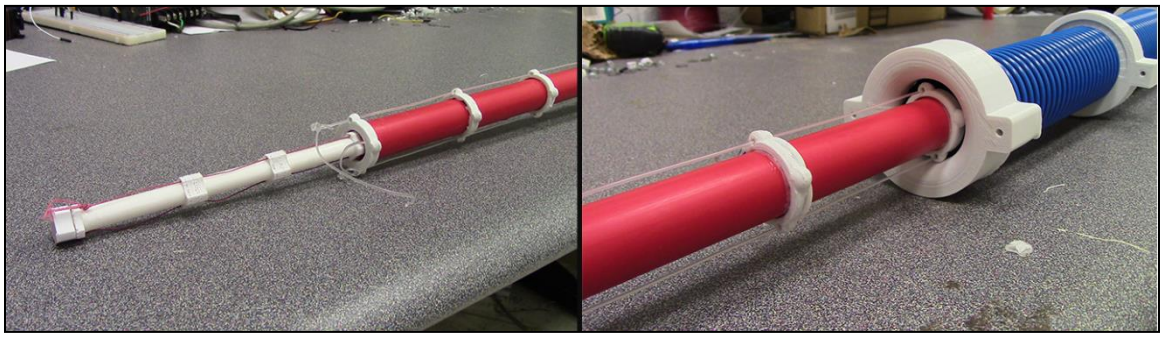

Figure 2.2. Initial model of tubes. Showing insufficient spacing between concentric tubes

Each section was designed to have two tendons routed through the spacers and terminating at the section end. With the selected sectional dimensions, the initially selected diameters (Figure 2.2) were found to be insufficiently spaced since the force required to pull the tendons was inordinately large - this was a tradeoff between relative stiffness of the sections and their maximum curvature. Another factor was the distance between the center of axis of the tube and the termination of a tendon on the spacer. As can be seen in Figure 2.3, the force required to bend the section reduces as the distance from the center of axis of the tube and the point of termination increases. The blue rectangles in Figure 2.3 are spacers and the red lines are tendons terminated at the end of the end cap (i.e. end spacer). It is assumed that the tube (black) does not have a pre-defined curvature and is equally pliable in all directions. When the left tendon is pulled, a higher force is required to bend by X°, as compared to the force required to bend by the same amount when the right tendon is pulled.

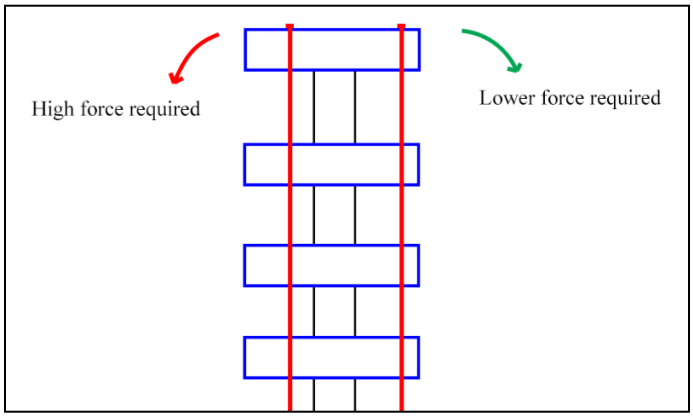

Figure 2.3. Torque based on axial distance

Because of this issue, it was decided to increase the diameters of the sections to 1/2” (0.025m), 2” (0.05m) and 4” (0.1m) for the distal, middle and proximal sections

respectively. However, with the section diameters having increased, their material properties changed as well.

The key difficulty in realizing the design is the inherent tradeoff between load capacity/backbone stability and workspace (achievable curvatures). Tests were performed with a large variety of flexible tubes [12]. Problems ranged from kinking in the tubes at high curvature to the inability to attain significant curvatures under reasonable actuation loads.

In order to achieve a greater curvature, a higher level of compliance was needed from the materials while also maintaining the backbone stability, i.e. sufficient stiffness to prevent kinking. PEX (cross-linked polyethylene) proved a suitable material for the distal section since at the diameter of ½" (0.02m), the bend achieved was sufficient for our requirements and the material was able to regain its shape upon release and relaxation of the tendons. As an alternative, CPVC tubes were also considered for the distal section. These tubes had higher stiffness and better payload capacity. They were also better at regaining their original shape after release and relaxation of the tendons. However, they had very low flexibility and the force required to bend the tubes by 90 degrees was upwards of 250 lbf (1112 N) which was causing the steel cable tendons used to snap and we were unable to obtain any conclusive results from the experiments. Another issue that arose because of such high application of force was warping of the 3D printed mounts (discussed later) which was misaligning the motors and causing damage to the components.

At larger diameters (>2", or 0.05m), achieving the necessary curvature became increasingly difficult, if at all, and resulted in kinking because of the required application

of a significantly higher force. As discussed in [2], materials with a high elastic strain are associated with a lower Young's modulus and for the desired application, a material with high elastic stress limits was needed.

After considering these factors, it was decided to experiment with PVC duct hoses for the middle and proximal sections. They had a considerable amount of stiffness and were reasonably pliable in their direction of inherent curvature. The PVC hoses used had a small predefined curvature to them, which is inherent in their manufactured state. This enables the tubes to be bent easily in one direction and be able to resist more load against that direction. The benefits from this property will be discussed in Section 3.1.

The middle section PVC tube selected had a bend radius of 6" (0.15m) and wall thickness of 0.055" (0.002m). It also had a smooth interior surface texture, which is desirable for actuation of the distal section inside it because the chances of the distal section getting caught at any point on the inner surface were reduced. For the proximal section, a PVC tube with a bend radius of 8"(0.2m) and wall thickness of 0.047" (0.0012m) was selected. The lower material thickness for this tube caused a problem of kinking in the material between spirals which is discussed later. A resulting successful prototype with these materials is shown in Figure 2.4 and Figure 2.5. Load capacity proved adequate, with bending angles (angles between base to tip tangents) of 90 degrees or more achieved.

Figure 2.4 Initial prototype while testing materials

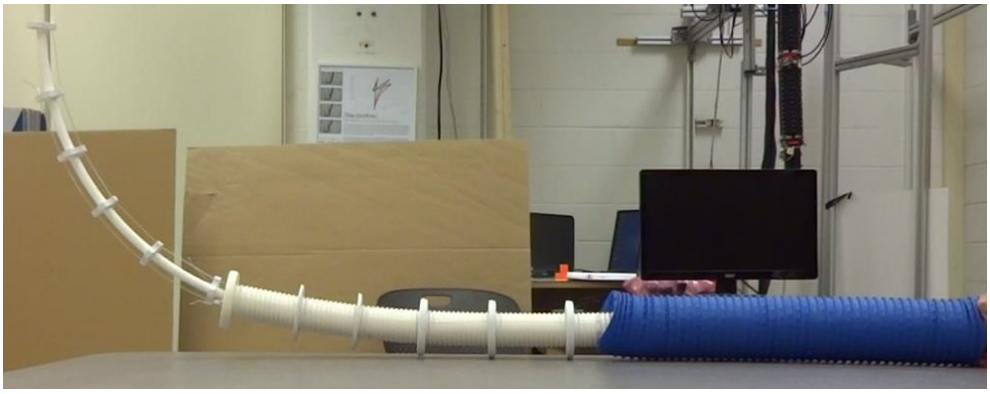

Figure 2.5 90 degree bend with the distal section

Characterization of the bending properties of the tubes was a design requirement. The tendons were aligned in the plane coincident with the slight bend inherent in the manufacture of these tubes. Figure 2.6 shows the results for bending with and against the inherent bend, for the middle section. Notice the bias in favor of actuating in the direction of the inherent bend.

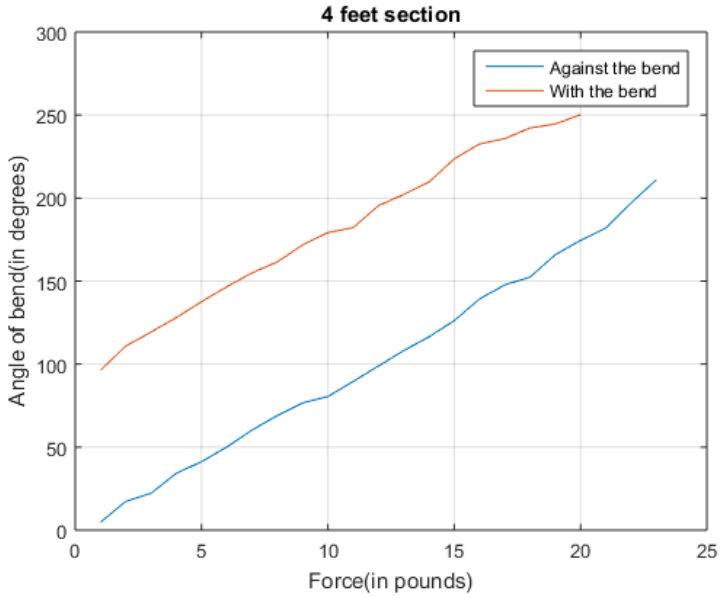

Figure 2.6 Actuator force versus bending in middle section

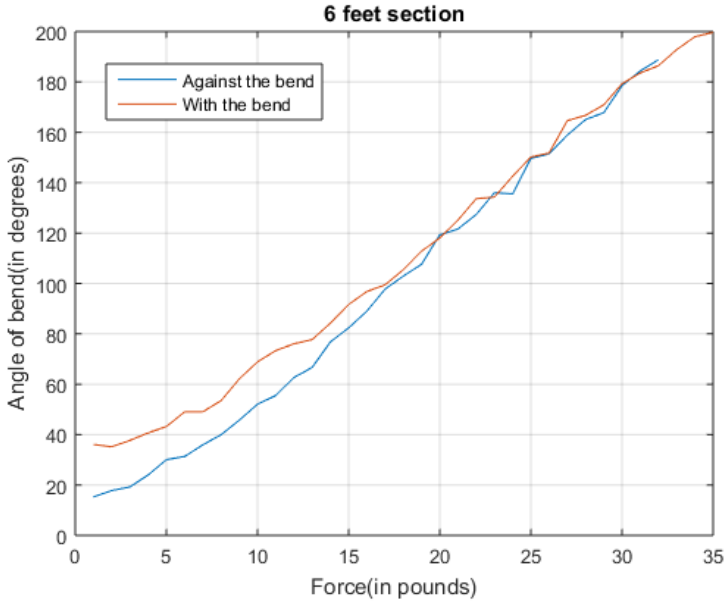

Figure 2.7 Actuator force versus bending in distal section

Figure 2.7 shows the equivalent result for the longer and thinner distal section. Notice in this case the effect of the inherent tube bend is less significant. Nevertheless, in operation the strategy adopted is to actively bend in the direction of (mechanical, via manufacturing) bending bias in the tube, and to only actuate in the opposite direction back to straight, i.e. zero curvature. Notice that since the tubes are rotated within each other by actuation at the base, the tubes only need to be bent in one dimension, with two dimensional bending of the backbone achieved by combinations of tube bending and rotation.

It was required to achieve linear as well as rotational actuation for the middle and distal sections. In order to facilitate this, the amount of friction between the tubes needed to be minimized. The initial approach considered was the use of linear rotary bearings along the inner part of the tubes, and covering each section with a smoother and flexible material, which would help in actuation. Linear rotary bearings have ball bearings on the inside, allowing for linear and rotational motion. The covering of smooth material on the outside of the tubes could create a surface for actuation and cover the spacers mounted along the length. The covering would also have to be flexible in order to not interfere with the bending (Figure 2.8).

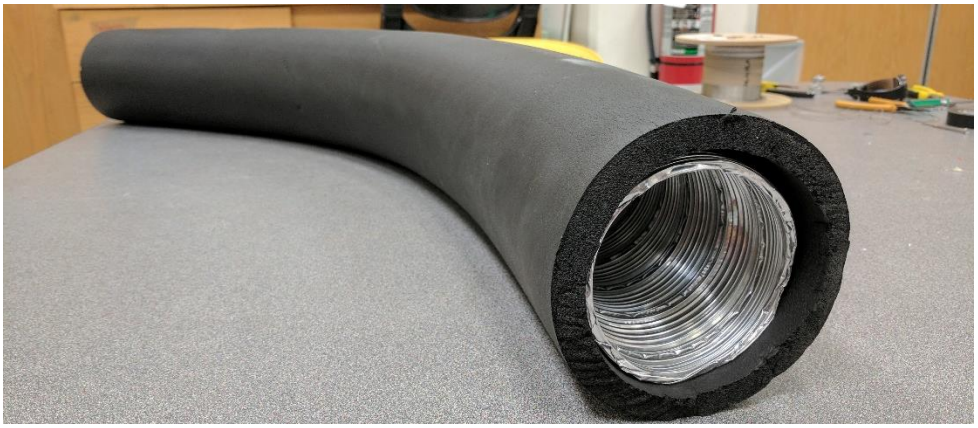

Figure 2.8 Smooth outer covering for the middle section

The outer covering would be smooth and there would be an inner shell for it, which would help the smoother and softer covering keep its shape. However, in order to implement this mechanism, it would have been necessary to further increase the diameters of the tubes and it proved difficult to find materials of the required dimensions while also possessing the physical properties we desired. It would also have reduced the bending of each section due to the covering on the outside of each section. Hence, we elected to use ball bearings.

2.3. Design for Spacers and Guides

As an alternative solution for the linear and rotational actuation issues, it was decided to integrate ball bearings in the spacers since they were already in use along the length of the tubes and provided sufficient support at every point of contact. This allowed us to reduce system mass while also reducing friction between the materials.

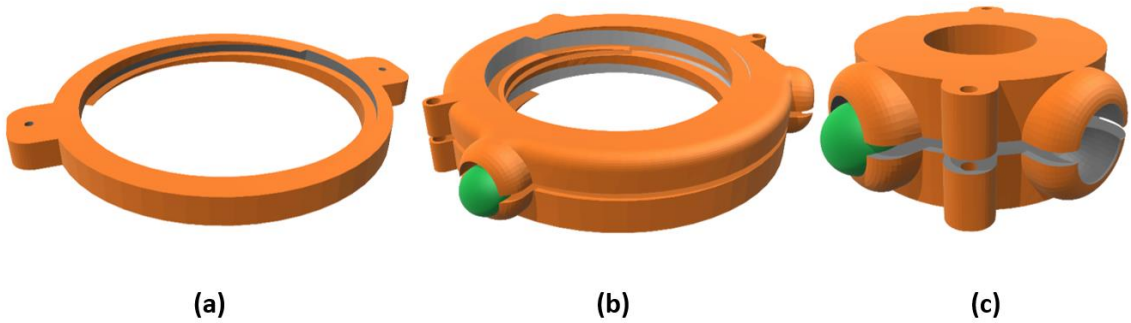

Figure 2.9 3D models of spacers with ball bearings (in green) (a) Proximal section spacer (b) Middle section spacer (c) Distal section spacer

To ensure smooth movement of the ball bearings, it was decided to 3D print the spacers. The spacers were designed in SolidWorks [13] and then exported to a 'gcode' format with the help of Cura [14]. Figure 2.9 (a), (b) and (c) shows the 3D designs of the spacers for the proximal, middle and distal sections respectively. In order to make the assembly easier, one spacer (for the middle and distal sections) was printed as two halves. After removing the support material and sanding, the ball bearings were placed at the respective slots and then the two halves of the spacer were glued together (Figure 2.10).

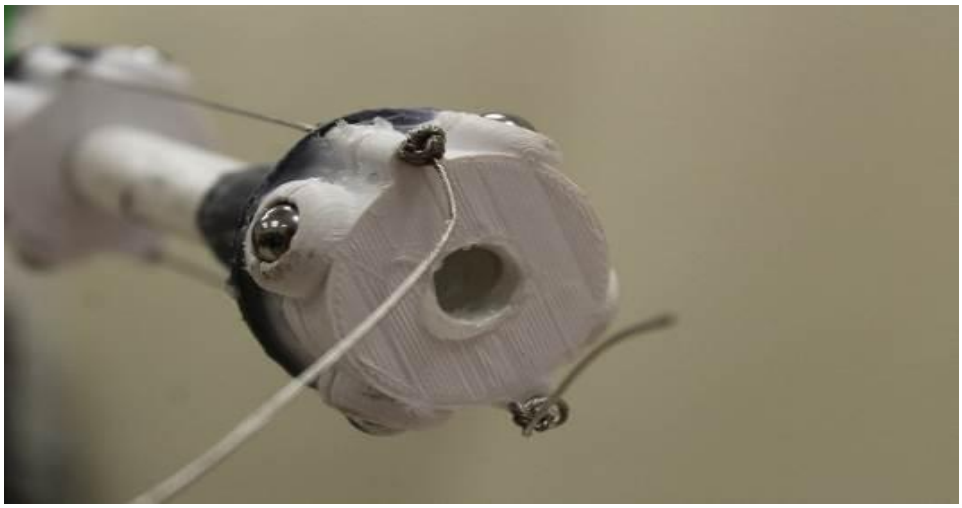

Figure 2.10 Distal section spacer with ball bearings

One disadvantage of having ball bearings on the spacers was that they added to the weight of the section and subsequently reduced the robot's payload capacity. However, they were deemed to be a necessity as this solution significantly reduced friction in tightly spaced situations of the type shown in Figure 2.11.

For the middle section, because there was threading on the outside of the PVC hose (Figure 2.12), the spacers were printed with threading on the inside so that they could be screwed on to the hose. This also helped in maintaining the spacers in their respective positions. To reduce the weight on the middle sections, it was decided to have only three ball bearings on the spacers since this was sufficient to keep the middle section centered inside the proximal section.

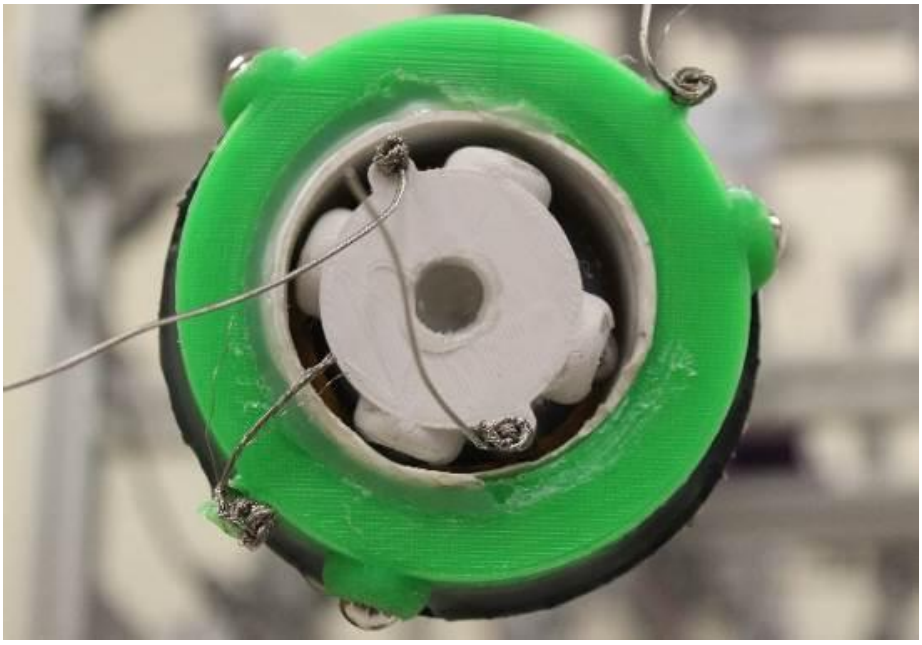

Figure 2.11 Spacing between middle (green) and distal (white) section

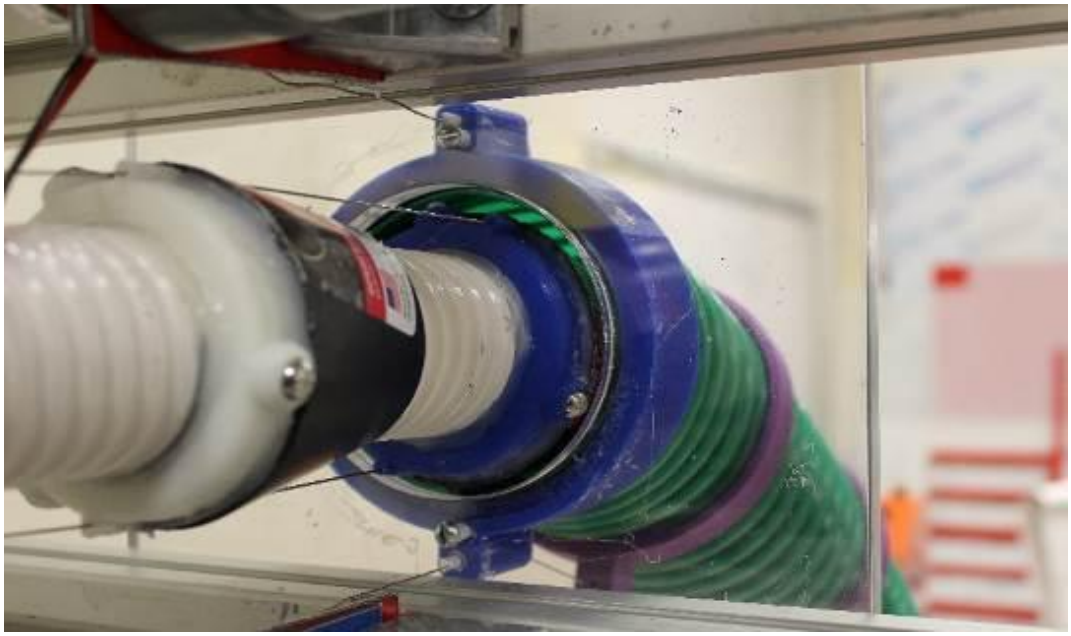

Figure 2.12 Middle section spacer entering the proximal section (dark grey-guides)

Because of the presence of spacers on the outside of the tubes, the surface created a non-ideal situation for linear tubular actuation, specifically, retraction of tubes into each other. Plastic ‘guides’ were added on the spacers as seen in Figure 2.11 so that during actuation, the ‘guides’ would align the inner tube with the opening of the outer tube. The ‘guides’ were simply plastic cones attached to the spacers in the direction of actuation and are illustrated in Figure 2.13.

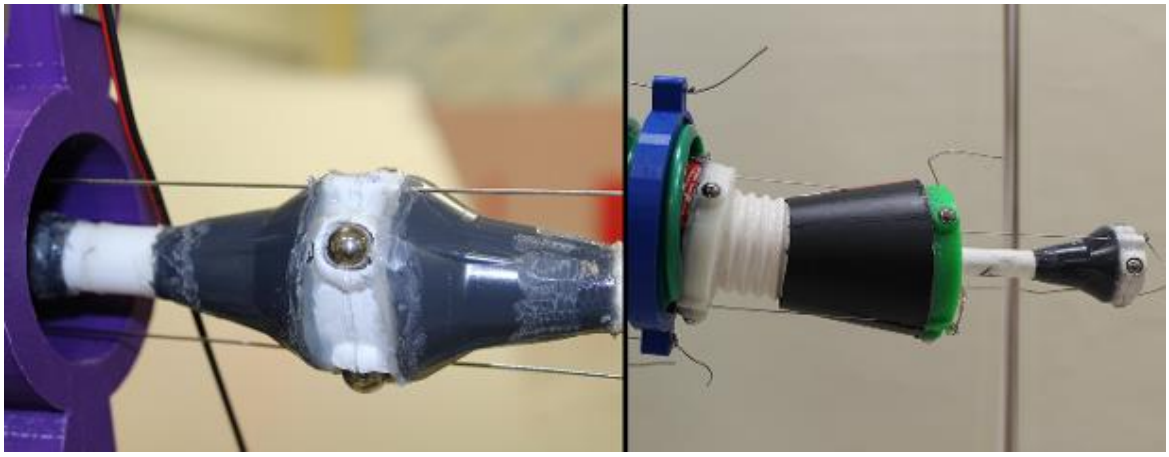

Figure 2.13 Conical guides for the tubes

As shown in the image on the right in Figure 2.13, some guides were mounted on the backside of the spacers since at those points, the spacers only needed ‘guidance’ when the tubes are retracting. In the image on the left side, the spacer has cones on both sides of the spacer since that spacer needed to be centered during extension as well as retraction. The guides were pieces cut out of long plastic funnels and their edges were smoothened in order to facilitate a smooth linear actuation.

2.4. Actuator Package and Mechanism

Having set up the tubes for actuation, a mechanism was needed to actuate the tubes. For linear actuation it was decided to use a simple rail-guide mechanism connected to a linear actuator. A similar mechanism was also used in [15], where an external actuator was used for linear actuation of the sections of a concentric tube robot. The base of each section was mounted on a ‘slider’ running on rails. The rail mechanism helped in creating a smooth and strong linear actuation mechanism. The rail made sure that the slider went parallel to the direction of actuation. Additionally, having support on the upper side of the slider

helped counteract the torque experienced during actuation. As shown in Figure 2.14, the base of each section was attached to a pillow block bearing which is mounted on the slider highlighted by green border.

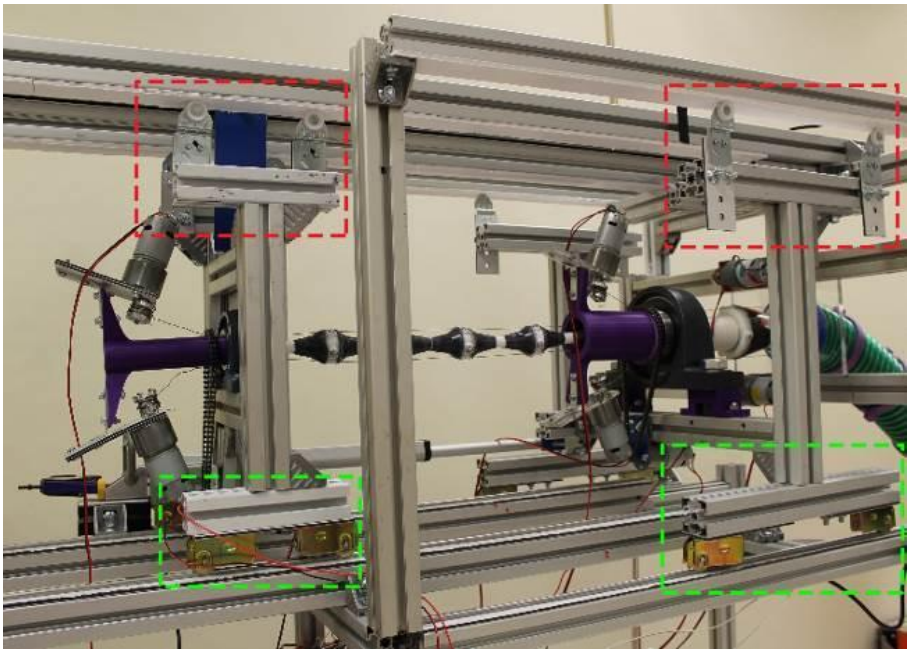

Figure 2.14 Mechanism for linear actuation. Upper rollers (in red), lower rail and rollers (in green)

Rollers were mounted on top of the slider (highlighted by the red border in Figure 2.14) for additional support and to prevent the assembly from toppling over. We used linear actuators capable of moving up to 150 lbs (68 kgs) to push/pull the sliders with speeds of about 1 inch/second (0.03 m/s). One drawback of this mechanism is that for the middle section to retract, the distal section has to be retracted first and similarly for the distal section to extend, the middle section has to extend first.

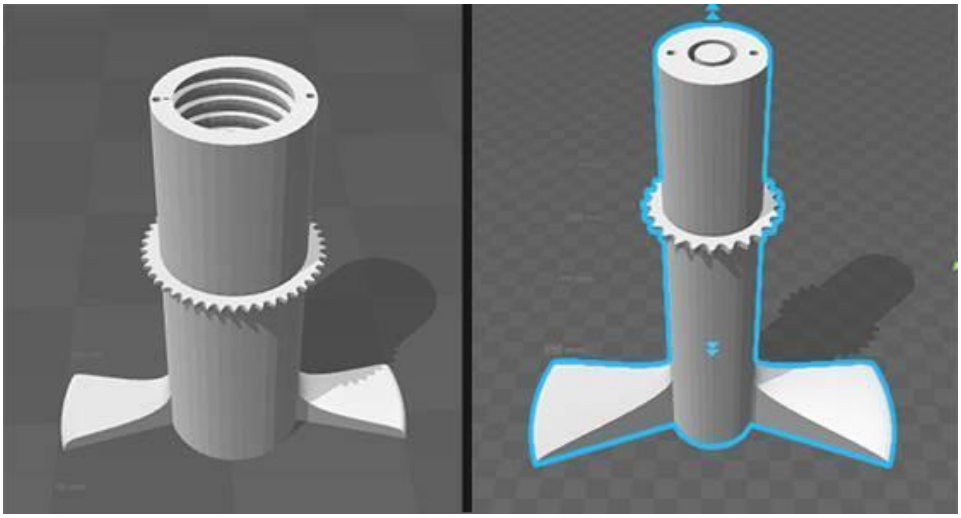

Figure 2.15 Mounts for middle (on left) and Distal (on right) sections

The base of each section was attached to 3D printed pieces (collars) shown in Figure 2.15, which facilitated rotational motion and had the tendon-pulling motors mounted on them. These collars were mounted on the pillow block bearings on the abovementioned sliders. These collars acted as connectors between the bearing and their respective sections. They were given a smooth outer profile in order to fit the pillow block bearing and sprocket teeth for connecting a #25 chain on the collars for rotational actuation. As seen in Figure 2.16, the collar for the middle section has threading on the inside matching the outer thread on the middle section hose.

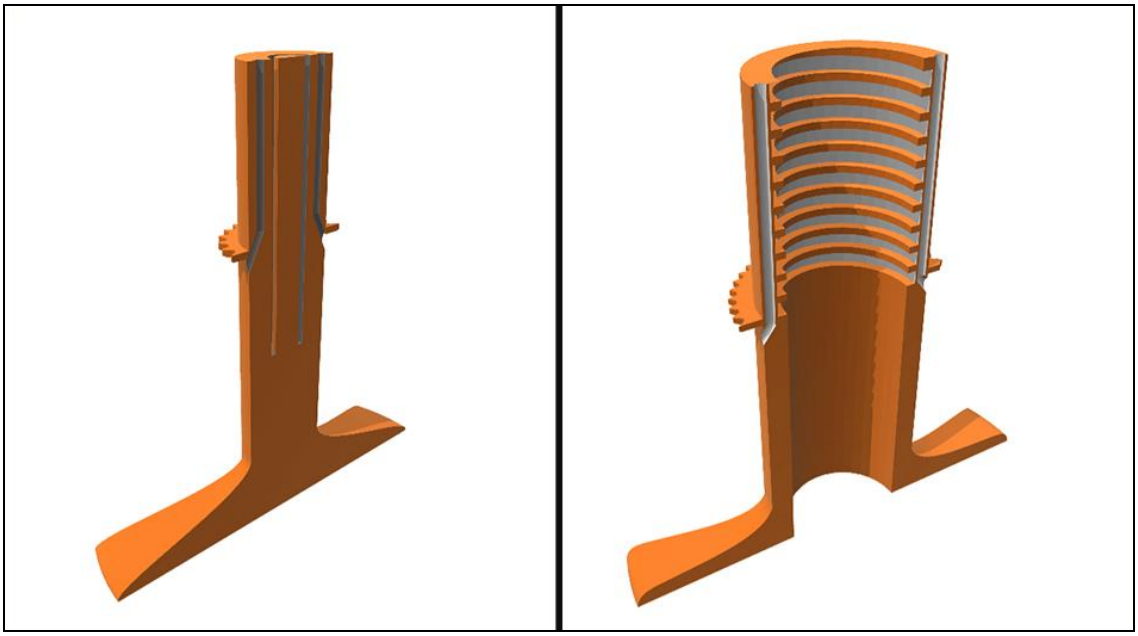

Figure 2.16 Section views of the Distal (left) and middle (right) collars

Also seen in Figure 2.16 is the slot in the distal collar for the PEX pipe to be fit into. There is a Sprocket for a #25 chain on each of the collars and two holes on the sides for tendons to pass through. These holes branch out from under the sprocket and the tendons passing through those holes are accessible to the motors as shown in Figure 2.16 and Figure 2.17.

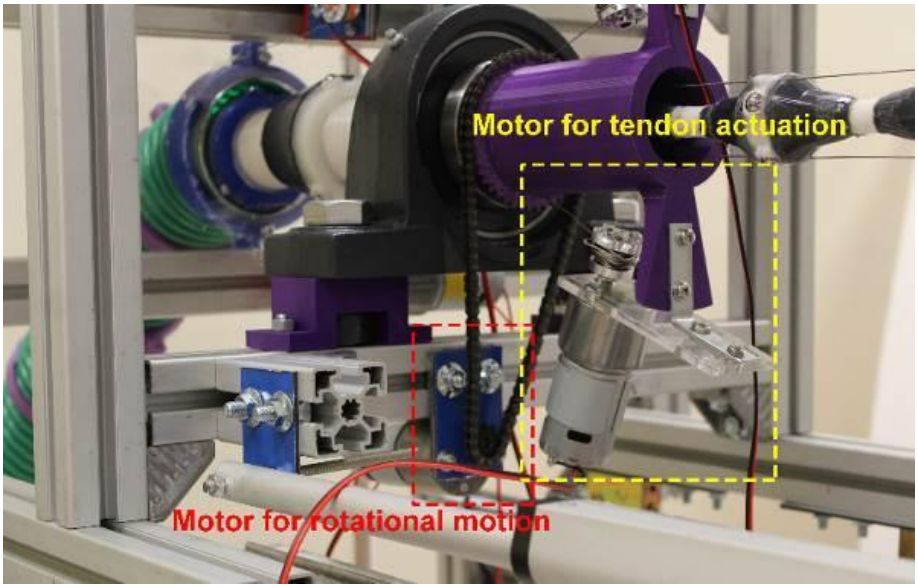

Figure 2.17 Motor placement (Middle section)

A motor mounted below the slider controls the rotational motion of each of the middle and distal section. The motor has a specialized attachment, enabling it to turn the section using the chain-sprocket system. Also mounted on the 3D printed collar are the tendon-driving motors. These motors are mounted at a 50° angle corresponding to the angle at which the tendons branch out from the collars. As has been mentioned above, the tendons branching out from the middle collar are connected to the tendon reels on motors. The distal section can also be seen (in Figure 2.17) entering the middle collar with the guides helping its linear actuation.

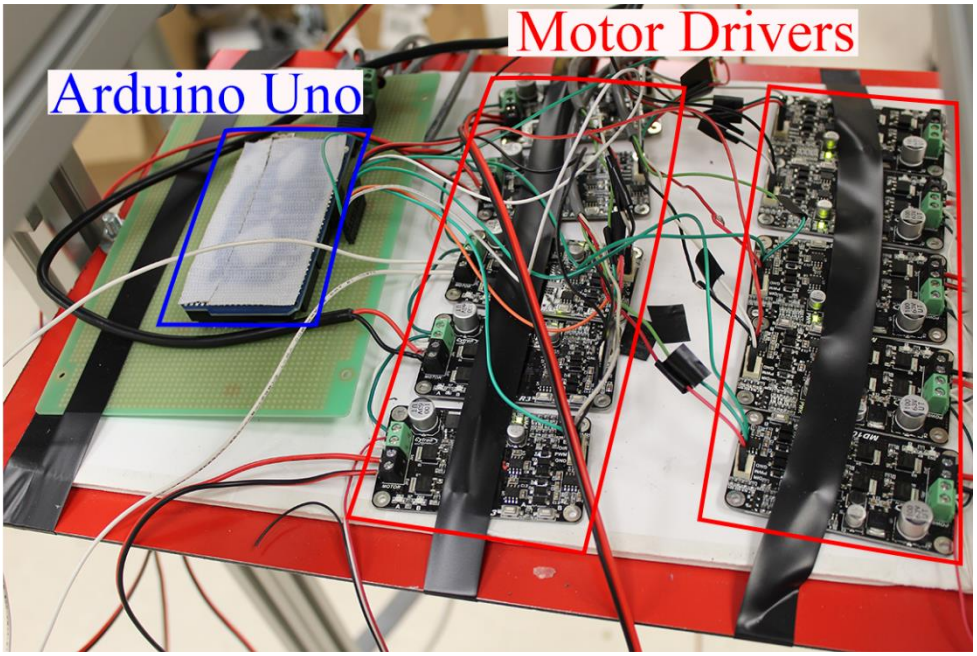

Figure 2.18. Motor drivers and Arduino with PCB

High torque motors were required for this application since the tension on the tendons would go up to 100-150 lbf (440 N) and the tendons selected were also to be of a similar load bearing capacity (~250 lbf). Each motor of the actuator package (including the linear actuators) is driven with the help of motor drivers and an Arduino Uno. The motor drivers used are Cytron 13A DC motor drivers with a voltage range of 5-25V. Each motor driver controls one motor and the PWM signals to the motor drivers are sent via an Arduino. A controller box of SPDT switches was made to control the winding/unwinding of the motors. Each switch controlled its respective motor and the up/down press of the SPDT switch sent the appropriate signal to the Arduino, which controlled the motors via the motor drivers.

To summarize, materials properties of the sections played a crucial role in developing a prototype of the design and hence selecting a suitable material was the first

step in building a working prototype. Once the material was chosen, spacer design and actuation mechanisms were designed to suit the chosen materials. The property of having an inherent bend (in the proximal and middle section) was also beneficial in obtaining better payload capacities and a larger working envelope. The spacer design was based on the external structure of each respective section and was aimed at providing a low friction medium between two sections. An important aspect of the spacer design was also to have the point of termination of the tendons as far away from the axis of rotation of the section as possible in order to achieve maximum bend for the respective section. The actuation mechanism was designed to minimize friction and make linear and rotational actuation as smooth as possible. Pillow block bearings used for relative rotational tube motion greatly reduced friction and provided a mechanically stable mount for their respective sections. A rail-guide mechanism also helped in creating a linear track for actuation and kept the sections aligned appropriately. While changes could be made to the design to improve the capability of the robot, the current physical structure of the prototype is fully functional for the proposed applications.

CHAPTER THREE: PROTOTYPE PERFORMANCE

The final prototype at full extension is shown in Figure 3.1. A series of tests were conducted to determine the capabilities of the robot. These tests included maximum bending and load capacity under linear actuation and rotational actuation. For these basic tests, the lengths of the proximal, middle and distal section were set at 2 feet, 3.5 feet and 5 feet respectively. Values for the maximum bend and load capacity change when the lengths of the sections are altered. For example, shorter lengths would produce better load capacities but lower flexibility and longer lengths would provide lower load capacity but higher flexibility. However, the above lengths were selected to be representatives of the average configuration space.

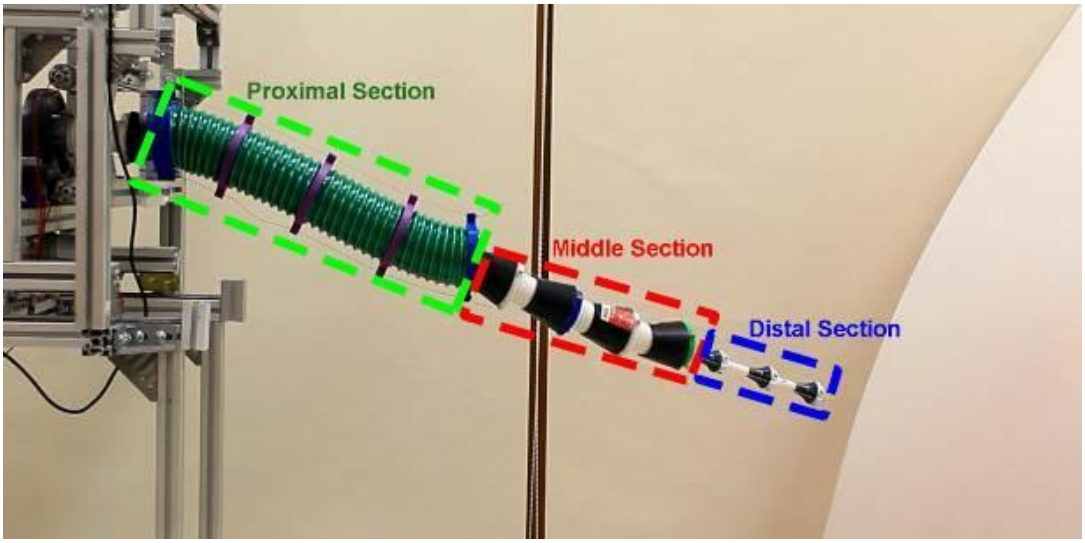

Figure 3.1 Final prototype with color coded sections

3.1 Bending Capabilities

In this test, the maximum bend a given section could achieve at the given lengths was evaluated. The bend was measured by degrees of deviation from the initial position and each section was bent until it displayed maximum bend without causing breakage or kinking.

The proximal section is a hose made out of PVC and its behavior is very much like a spring with properties of low compliance and high compression, the effects of which can be seen in Figure 3.2. Because of these materials properties, when the tendons for the proximal section are pulled, because of the weight of the other two sections bearing on it, the extent to which the proximal section can bend is reduced and the tube tends to compress. When attempting to bend the proximal section by a large amount, ‘folds’ are created between the material of the tube, making linear actuation difficult.

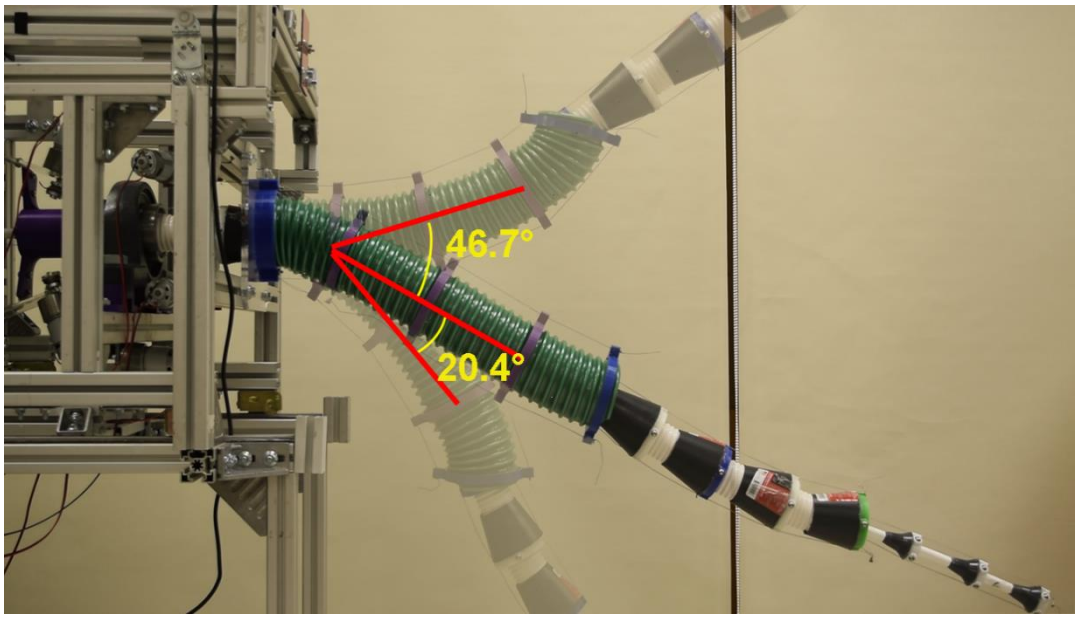

Figure 3.2 Maximum bend for proximal section

It was observed that the proximal section, without external load, could achieve an angle of elevation of 46.7° with maximum angle of depression of 20.4°. These are the maximum limits of the section without any bending of the other two sections. These observations were made assuming that all sections are extended to their maximum lengths. This demonstrates that the proximal section can be effectively used to lift and deploy the other two sections to an appropriate height and provide support for them. As seen in Figure 3.2, the bending observed in the direction of inherent curvature is greater than the bending observed against it as might be expected.

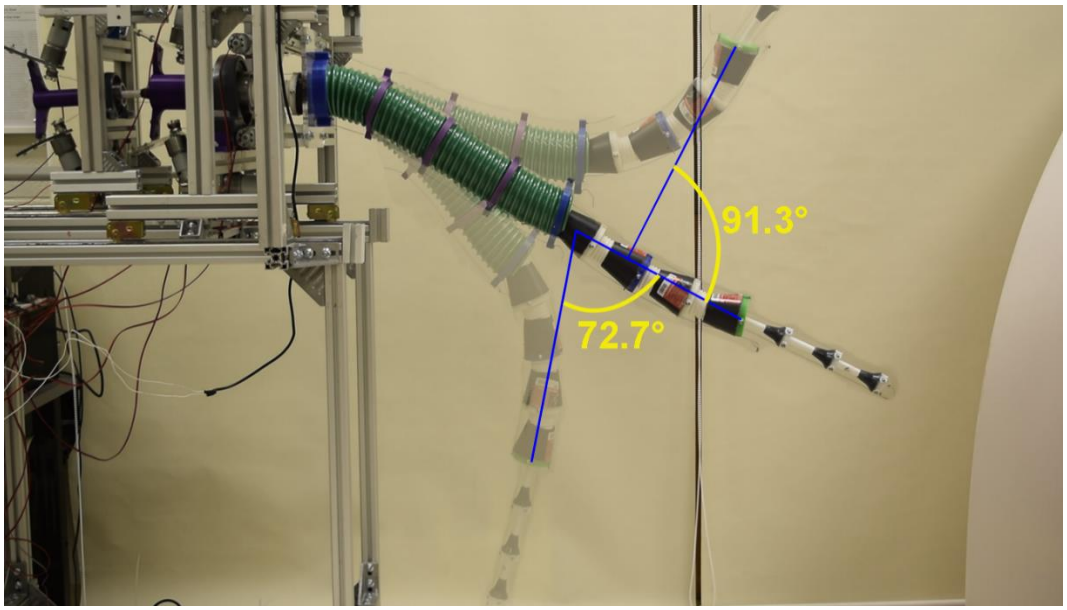

Figure 3.3 Maximum bend for middle section

As stated previously, the middle section comprises a tube with a thicker wall, resulting in the section being less prone to kinking and thus, enhancing its flexibility. It has a predefined bias curve due to its manufacture resulting in the bending conditions being different when working with or against its predefined shape. As can be seen in

Figure 3.3, while bending the middle section, the proximal section also gets pulled in the direction of the bend due to the inherent coupling between the two tubes. Being more flexible as compared to the proximal section, the middle section has a greater working envelope and can achieve 91.3° planar bends 'with the curve and 72.7° 'against the curve'. The difference in the two cases is the force required to achieve bending. Bending against the predefined curve puts a significant amount of stress on the motors and any additional force applied on the tendons caused the spacers and tendons to break because of the applied stress in some situations.

The situation and observations were different for the distal section, due to its significantly different material properties. The PEX pipe did not have a predefined bias bend to it and was equally pliable in all directions. It was, however, prone to acquiring an inherent bend to it when under stress for longer periods of time, but would eventually regain its naturally linear shape. It was able to achieve a 187.9° arc when bending (Figure 3.4).

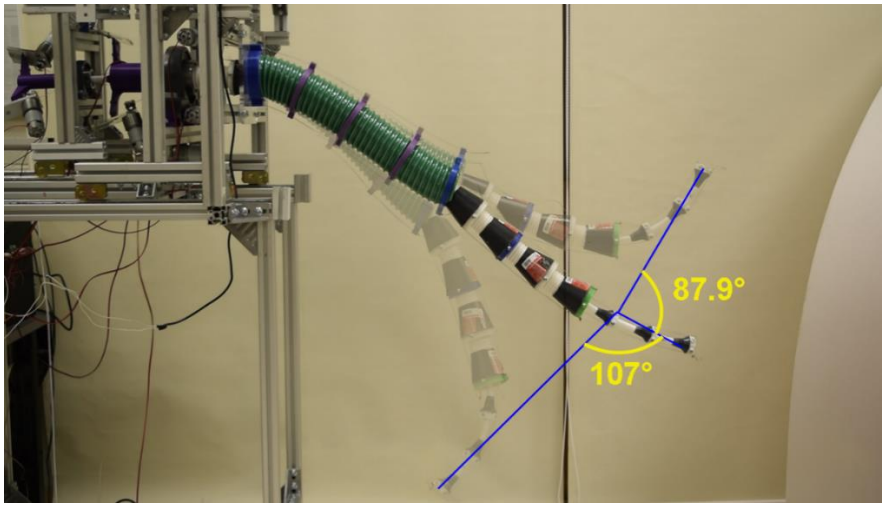

Figure 3.4 Maximum bend for distal section

The bending observed when lifting the distal section was observed to be lesser than that observed when the robot was being pushed down. This was an effect of gravitational loading acting in favor of biasing the robot towards the ground. Further bending was found to damage the pipe structure due to surpassing its yield point or elastic limit and was thus avoided.

3.2 Load Tests

In order to demonstrate the load carrying capacity of the robot, we attached a series of loads at the ends of each section to measure the deviation in their structure. The sections were aligned in order for them to be completely horizontal (worst case against gravity). Then a load scale was attached at the ends of each section and the angle deviation at equally spaced steps was recorded.

For the proximal section, the load capacity was found to be significantly higher than the other sections. The maximum load it could lift was 11 lbs. For the maximum load, the angle deviation was found to be 19.1° (Figure 3.5).

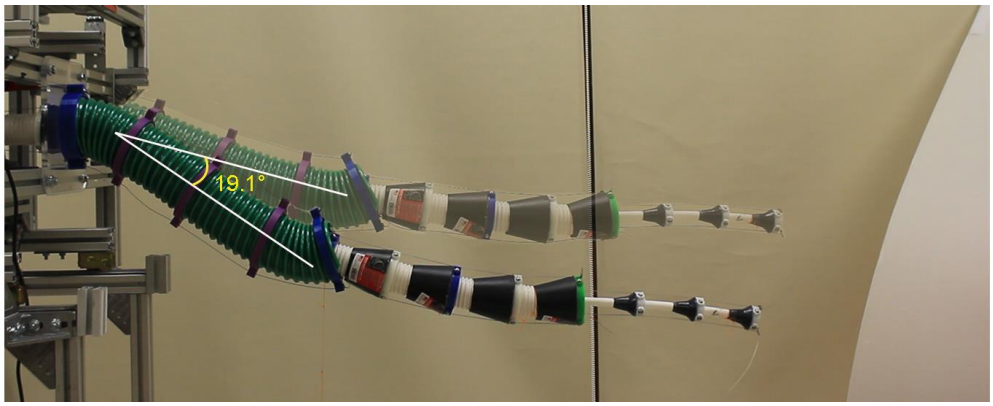

Figure 3.5 Angle deviation of proximal section at maximum load

Table 3.1 represents the readings taken while performing the load tests for the proximal section.

Table 3.1 Load test of Proximal section

Force (N)	Angle (degrees)
5 (1.12 lbs.)	3
10 (2.24 lbs.)	6.2
15 (3.37 lbs.)	9.5
20 (4.49 lbs.)	11.5
25 (5.62 lbs.)	13.9
30 (6.74 lbs.)	15.4
35 (7.86 lbs.)	16.3
40 (9 lbs.)	17
45 (10.11 lbs.)	18.1
50 (11.24 lbs.)	19.1

The above readings were taken with the inherent bend of the tube facing up, i.e. the loads were applied against the bend of the proximal tube. The proximal tube was attached so that the inherent bend is always facing upwards. This was done to improve the load capacity of the robot while maintaining the robot's ability to access the desired area of operation.

For the middle section, the maximum load it could lift was 8 lbs. This was still relatively large but with a larger angle deviation of 28.6° (Figure 3.6). The middle section was also oriented with the inherent bend facing upwards (i.e. easier to bend upwards).

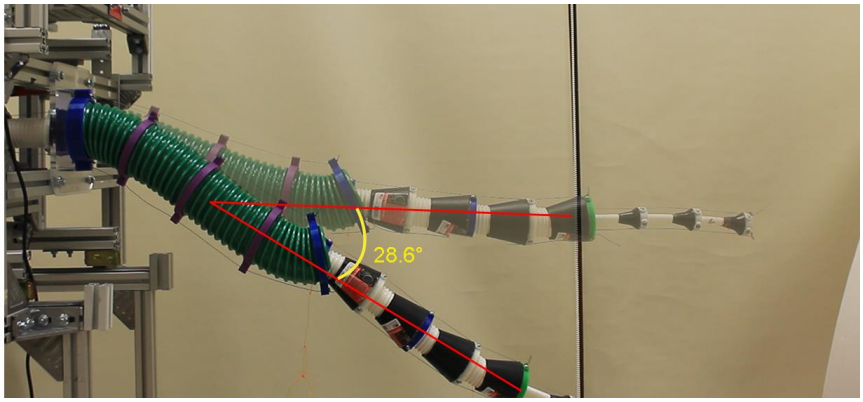

Figure 3.6 Angle deviation for middle section at maximum load

Table 3.2 details the readings taken while measuring the maximum load capacity for the middle section.

Table 3.2 Load test for Middle section

Force (N)	Angle (degrees)
5 (1.12 lbs.)	2
10 (2.24 lbs.)	6.3
15 (3.37 lbs.)	11.3
20 (4.49 lbs.)	16.6
25 (5.62 lbs.)	20.9
30 (6.74 lbs.)	24.5
35 (7.86 lbs.)	28.6

For the distal section, the maximum load it could lift was 2.5 lbs. and the deviation was the largest among the three sections, namely 30.2° (Figure 3.7). While the load capacity of the distal section was the lowest, it is also made up of the thinnest and the least stiff of the three materials. On the other hand, it is the most flexible of the sections.

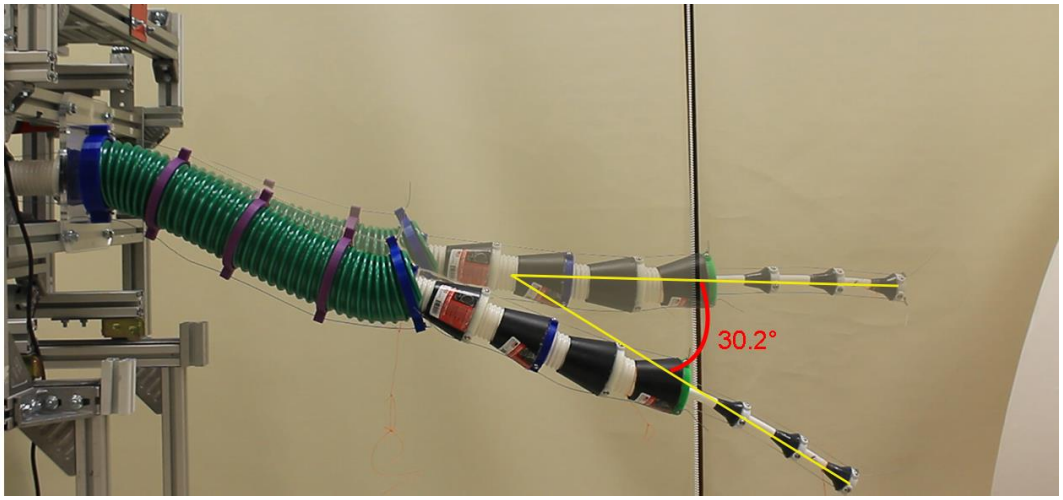

Figure 3.7 Angle deviation for distal section at maximum load

Table 3.3 Load tests for Distal section

Force (N)	Angle (degrees)
1 (0.2 lbs.)	4.6
2 (0.44 lbs.)	5.9
3 (0.67 lbs.)	8.4
4 (0.89 lbs.)	10.5
5 (1.12 lbs.)	12.7
6 (1.34 lbs.)	16.7
7 (1.57 lbs.)	19.2
8 (1.79 lbs.)	21.8
9 (2.02 lbs.)	24.4
10 (2.24 lbs.)	27.3
11(2.47 lbs.)	30.2

It can be observed from the performance of the prototype that while the dexterity of the robot is as per our initial assumptions, the load capacity needs to be improved for the distal section and possibly for the remainder of the robot. The angles of a sector covered

by the sections were 67.1°, 164° and 194.9° for the proximal, middle and distal section respectively. As mentioned before, these are as based on requirements, as the sections serve different purposes, with the proximal section providing the maximum load bearing capacity and having enough dexterity to raise/lower the other two sections, the middle section helping direct the distal section to the appropriate direction and having a relatively higher load capacity and the distal section having the maximum amount of dexterity in order to access difficult to reach areas.

CHAPTER FOUR: EXPERIMENTAL EVALUATION

Systematic experiments were conducted with the robot to test the motion envelope of each of the three sections. An important factor to consider was the inherent bend bias that the sections have because of the way they have been manufactured and stored. While the inherent bend in a section limits its range of motion, it can also provide necessary resistance/compliance in order to achieve the required position of the tip. An advantage that continuum robots have over rigid link robots is the ability to reach difficult to access areas and perform a desired task. Following the results from the maximum bend and horizontal load tests, it was decided to perform two main demonstration tasks with the robot. Experiment 1 covers cleaning a simulated 'glove-box' primarily used for Nuclear waste handling. This was to demonstrate the ability of the robot tip to access any desired location in the given 3D space (within its working envelope). Experiment 2 was designed to demonstrate a remote inspection application where the robot was tasked with attempting to inspect an object hidden from plain sight.

4.1. Experiment 1 [16]

The aim of this experiment was mainly to demonstrate the use of a robotic system for maintenance and remediation in a 'glove-box' type environment typically used in nuclear radiation remediation. Glove boxes are sealed containers built to perform radiation based experiments in. These glove boxes do not offer a great amount of shielding for the operator and they are not built to handle high gamma or high neutron sources. Remediation and maintenance of such containers are very hazardous tasks for humans to perform and a use of a dexterous continuum robotic system would be an ideal application for them.

For the experiment, a mockup of a glove box was created to demonstrate the ability of the robot to be able to clean all faces of the container with the help of an attachment at its tip. The glove box was sized to be 44 in x 44 in x 32 in (l x b x h) (Figure 4.1). The walls were made of acrylic sheets and were selected to be transparent for demonstration purposes. A bristled fan cleaner was attached at the tip of the distal section to simulate a cleaning attachment for the maintenance of a glove box.

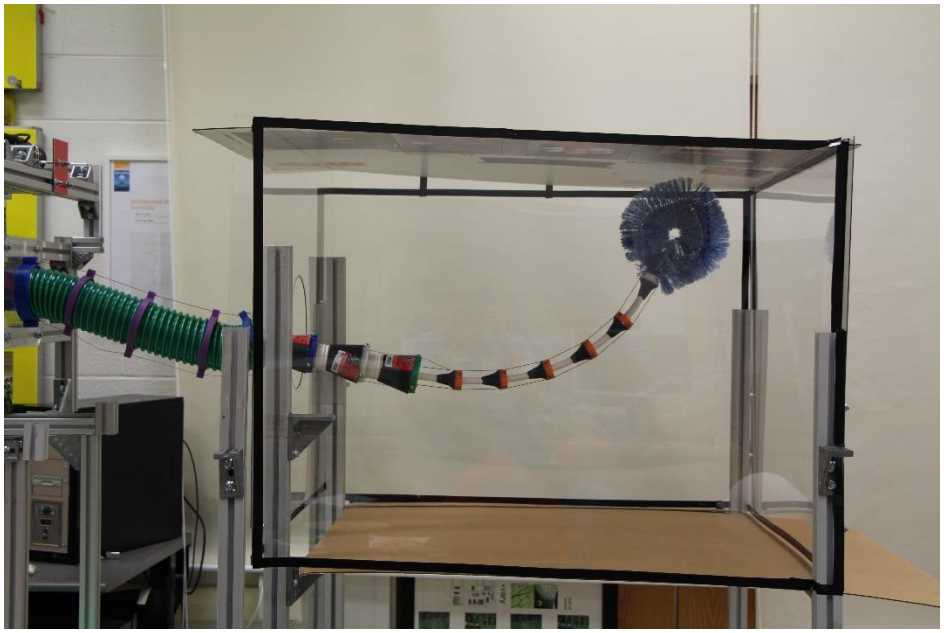

Figure 4.1 Glove box cell

The distal section used for this experiment was extended to 6 feet in length to increase the reach of the robot. The material properties of the middle section helped provide support to the distal section enabling it to reach higher spots. Having an inherent bend in the middle section was helpful in achieving a 180° bend in order to reach the back walls of the cell. This was achieved by bending the distal section in the direction of the inherent bend of the middle section. The proximal section helped in bringing the other sections to

an appropriate height and help them enter the cell through a 7.75 inch diameter hole on the front face (Figure 4.2).

Figure 4.2 Robot entering the cell through a 7.75 inch hole

The robot was mounted on a mobile trolley able to be pushed manually. To demonstrate a sweeping action, the tip of the robot made contact with a face and the trolley was then pulled back. To demonstrate to robot's ability to reach all points in the cell, all corners of the cell were accessed as a sufficient proof for being able to access any other point in the cell. (Figure 4.3 and Figure 4.4)

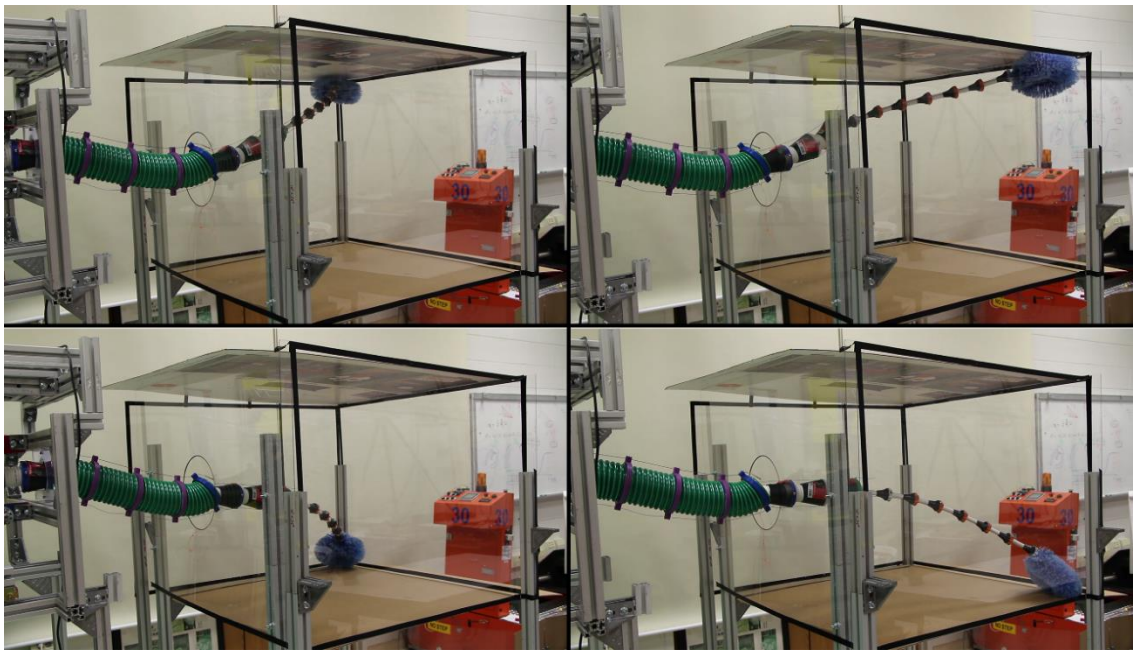

Figure 4.3 Accessing the back four corners of the cell

As can be seen in Figure 4.3, for accessing the farther end of the cell, the proximal section was lifted in order to help the distal section maintain the required height. Additional support was provided by the middle section to direct the distal section in the desired direction. The points interior to the box were easily accessible with minimal bending of the distal section. With the help of the built-in rotational motion, the distal section was rotated to orient the tendons in the desired direction of motion and subsequent pulling of the appropriate tendon helped achieve the given task.

Accessing the front face of the cell required a more complex combination of movements from the three sections (Figure 4.4). The proximal section played an important role in this task as it provided the support that the middle section provided in the previous task by lifting the other two sections to an appropriate height.

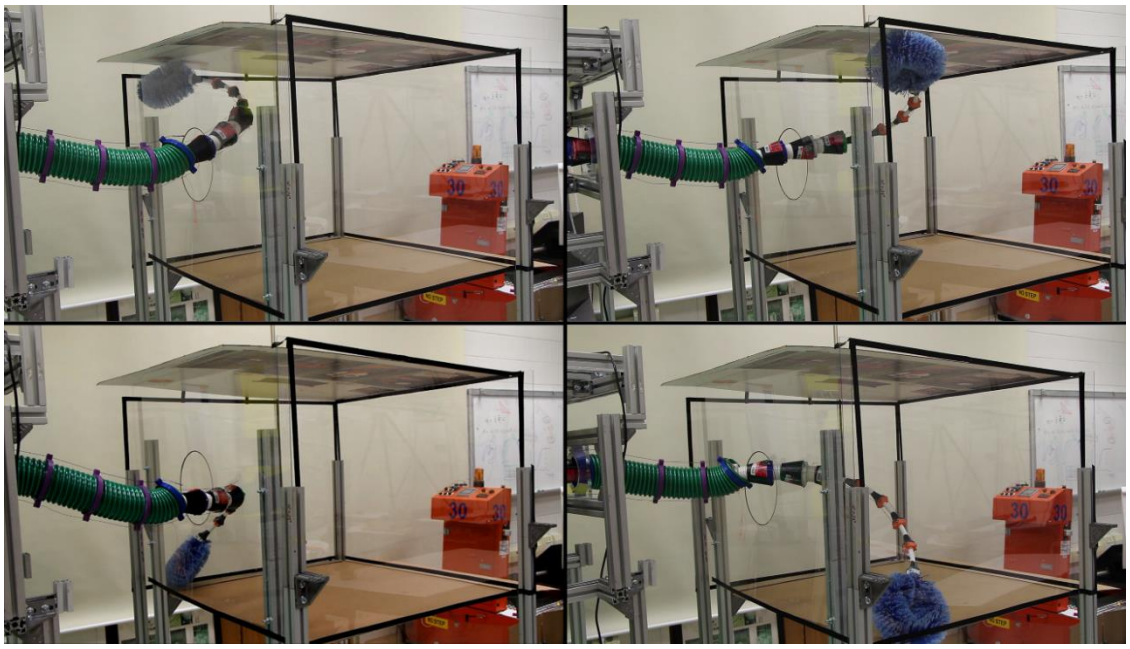

Figure 4.4 Accessing the front four corners of the glovebox cell

The middle section was rotated to orient the side with the inherent bend toward the corner that was to be accessed. The distal section was then bent towards the corner to be accessed. While this worked smoothly for the bottom two corners, a slightly different approach was used to access the top two corners. After the inherent bend of the middle section was oriented towards the corner, the tendon on the opposite side was pulled to enable the distal section to take a larger radius of curvature while bending towards the corner. Because of the effects of gravitational loading, the sections experienced torque along their length and its effect was reduced by adjusting the orientation of the respective section with the help of rotational motion.

Hence, the robot was able to access all the extremities of the constructed glovebox cell and would be equally capable for gloveboxes of a similar size and dimensions. The physical dimensions of the robot can be scaled up/down as needed. For a larger/smaller

glovebox, the lengths of the sections can be adjusted to effectively access all corners of the container. Hence, from this experiment we can conclude that the TREE design can act as a successful robotic system for the maintenance and remediation of a glovebox cell in a hazardous environment.

4.2. Experiment 2 [17]

In addition to reaching a specific point in 3D space with the tip, we wished to demonstrate the ability of the robot to maneuver through tight non-linear spaces and perform remote inspection tasks. The aim of the experiment reported in this subsection was to inspect an object which is hidden from plain sight.

This experiment was performed in two parts. The first one required the robot to enter a 5" pipe and then perform a 90° bend to view the object (a toy pumpkin) (Figure 4.5).

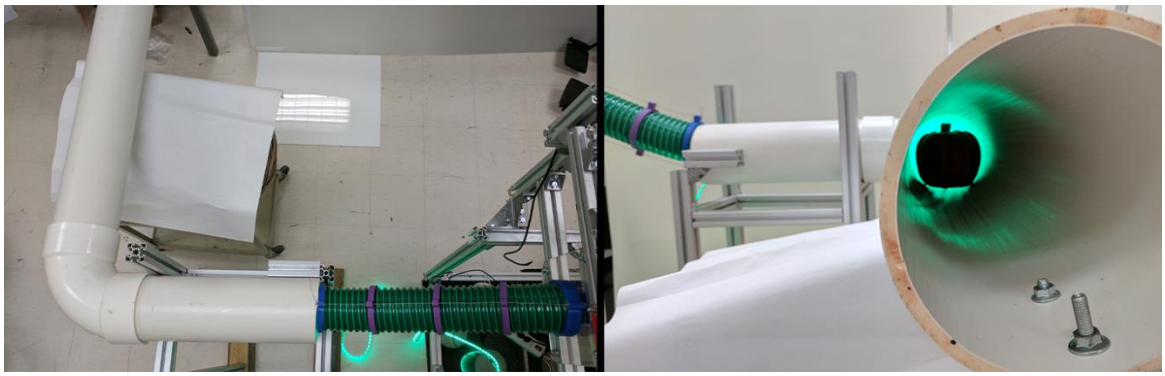

Figure 4.5 Experiment setup (Pumpkin object on the right). Left: Top view, Right: side view (from top of left image)

The robot extended 1.8 feet into the pipe and then bent to the right to view a toy pumpkin with illuminated eyes. The entire robot assembly was mounted on a mobile base which can be moved on flat surfaces in order to orient the robot as required. The distal

section had a camera attached to its tip enabling visual feedback and hence teleoperation of the robot inside the pipe. The first step was to move the base towards to pipe in order to get the sections appropriately oriented to the entrance of the pipe. The proximal section was actuated downwards in order to align the middle section with the tube entrance.

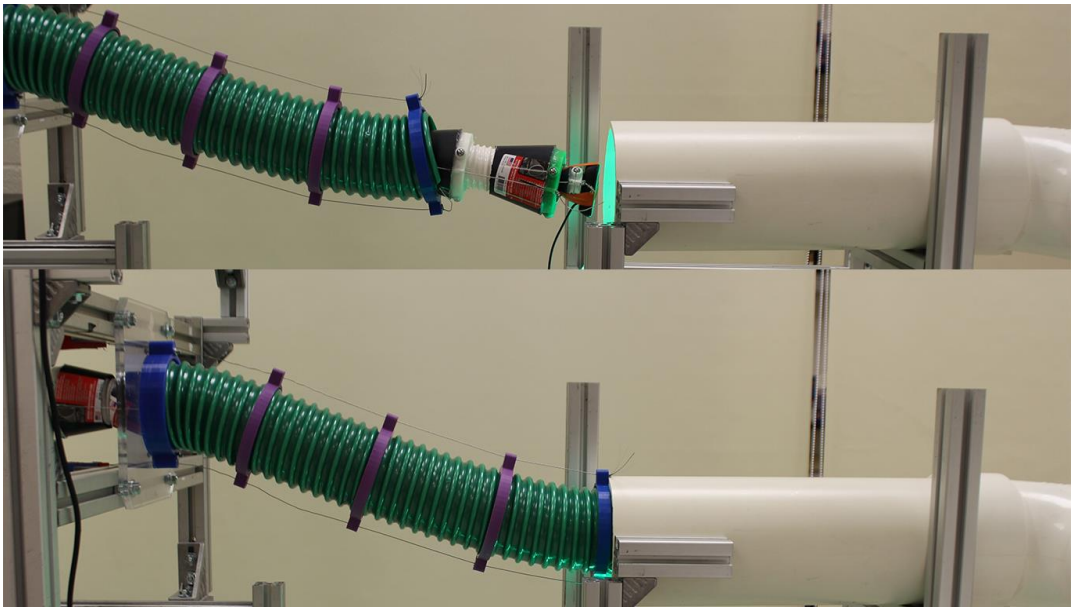

Figure 4.6 Alignment of the tip with the pipe entrance

Once the tip of the middle and the distal sections were properly aligned, we extended the middle and distal sections inside the tube simultaneously (Figure 4.6). This was done by observing the movement of the sections through the camera mounted on the tip of the distal section. Once the section reached the appropriate depth, the distal section was bent and after the tip section worked its way around the bend, the pumpkin inside the tube could be clearly seen (Figure 4.7).

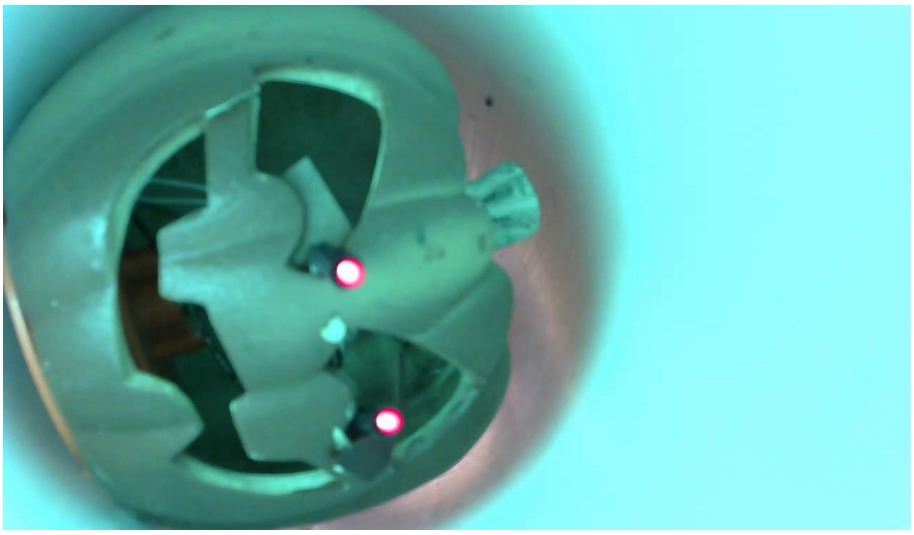

Figure 4.7 Image of pumpkin from camera on distal section

As an additional task, we attempted to increase the complexity of the field and make the robot go through tubes at different heights and still be able to perform a 90° bend to view an object. The setup is shown in Figure 4.8.

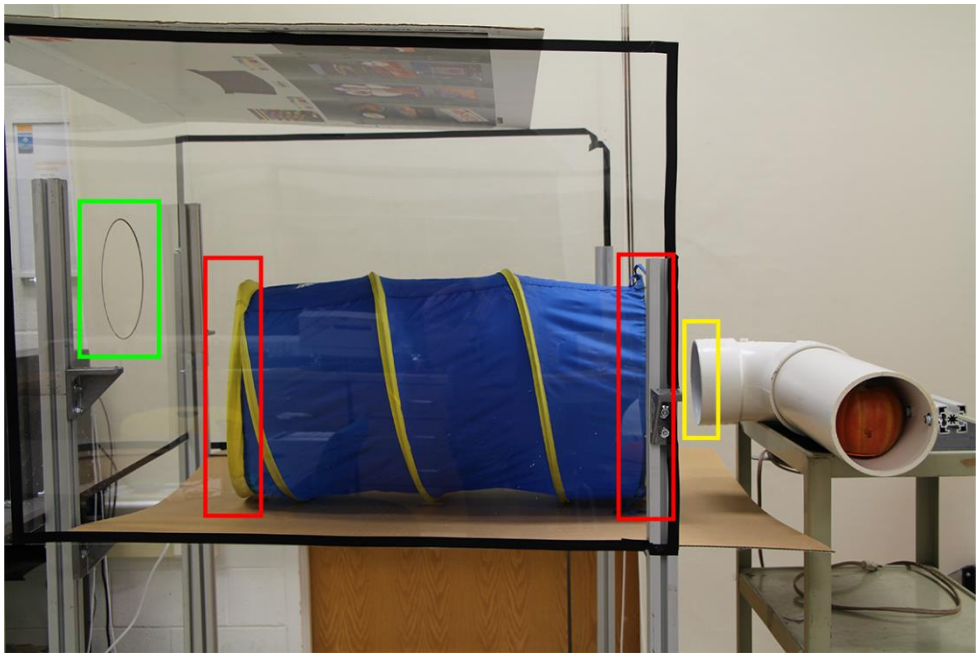

Figure 4.8 Green - Entrance 1, Red - entrance 2 and exit, Yellow - entrance 3

As seen in Figure 4.8, the robot needed to enter through the 9.75 inch hole highlighted by the green rectangle, then lower itself into the entrance highlighted by the red rectangle and then enter the 5 inch diameter pipe highlighted by the yellow rectangle. After having entered the pipe, the robot needed to perform a 90° turn to view the toy pumpkin hidden inside the pipe. The distal section used for this experiment was longer in length (6 feet) and had a camera attached at its tip.

The robot assembly was mounted on a mobile trolley and was moved on a flat floor in order to align the robot with Entrance 1 and enter it. The distal section was then extended inside the cell and into Entrance 2 with help from the middle section which was bend slightly downwards to get the appropriate orientation. With the simultaneous linear actuation of the middle and distal section, the robot extended its reach towards Entrance 3. (Figure 4.9)

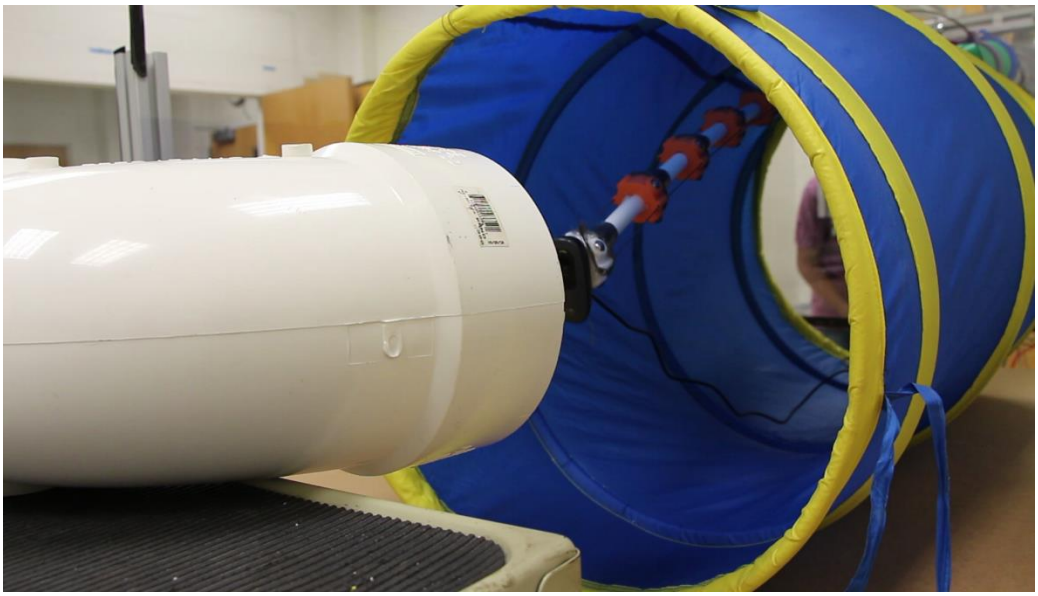

Figure 4.9 Distal section (with tip camera) entering the pipe

Subsequent bending and rotation of the distal section was required to direct it towards the entrance of the pipe. The middle section also played an important role in providing support to the distal section. Once the distal section entered the tube, it was rotated and bent 90° to view the toy pumpkin (Figure 4.10).

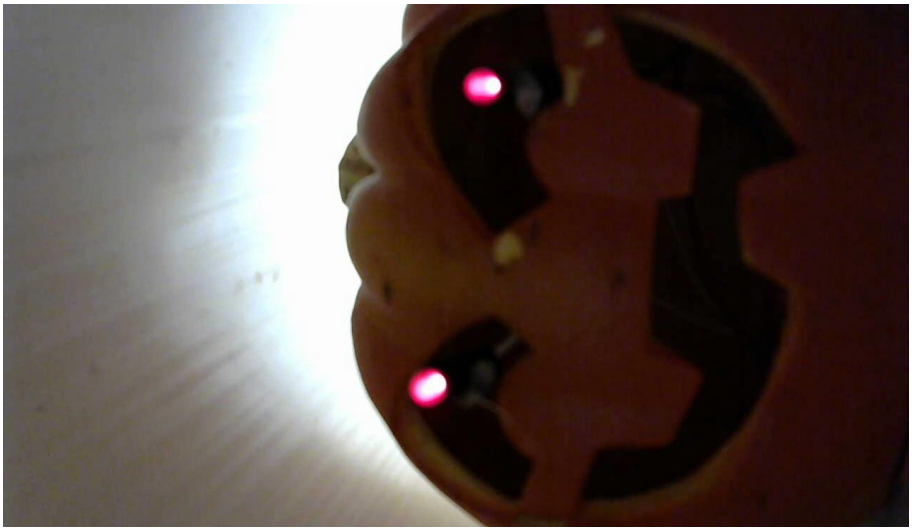

Figure 4.10 Toy pumpkin viewed from a tip camera on the distal section

Hence, we effectively demonstrated the robots ability to successfully reach into and explore areas which are difficult to access. The three sections of the robot can be used together to perform remote inspection tasks effectively. The primary issue during the task was the torsion that acted on the sections. This effort caused a bent section to drop a few degrees below its intended orientation and made it difficult to control the robot when it was not completely visible. This effect may be reduced with either using a stiffer material, section shape feedback or having additional tendons along the length of the section specifically to counter-act the torsion. However, after experimental evaluation, it can be concluded that the robot behaved as expected and performed the given tasks successfully.

CHAPTER FIVE: CONCLUSIONS AND FUTURE WORK

5.1 Conclusions

This thesis introduces a large-scale hybrid continuum trunk robot with a concentric tube design. The work is specifically aimed at applications where long continuum robots are required with higher payload capacities as compared to thin vine-like continuum robots. It is the first example of a large scale concentric tube design which was earlier primarily used for medical applications.

In this thesis, we showed how concentric tubes of appropriate lengths and materials can be used at a scale of about 6 feet in length to build functional continuum robots. The overall length of the sections of the robot varied as per their applications but were of a similar maximum range (5-6 feet). Concentric tubes also provided sufficient structural support for applications where linear actuation of independent sections was required. The design was also capable of rotational actuation which helped reduce the number of tendons in each section, subsequently reducing the number of motors used per section.

An important factor which enabled smooth linear and rotational actuation in the tubes was the innovative design for the spacers and guides. Ball bearings on the outside of the spacers and smooth interiors of tubes provided a low friction mechanism for actuation. With the external spacers, linear actuation was a potentially significant challenge but plastic guides attached to the spacers helped accurately orient the sections and maintain the spacing between tubes necessary for linear motion.

A smooth mechanism for the linear and rotational motion was built with the help of low friction pillow block bearings (for rotational motion) and rail guide mechanisms

(for linear actuation). Linear actuators were attached to the sliders as detailed in section 2.3, and 3D printed collars acted as effective connectors between the pillow block bearings on the sliders and the concentric tube sections.

The load capacity of each individual section was measured with the proximal section having the highest load capacity and the distal section having the lowest, as expected. The purpose of the proximal section was primarily to lift majority of the loads and be able to adjust the height of the other two sections effectively. The distal section was designed to have high dexterity and compliance in order to better manipulate through difficult to access areas. This was also observed during the measurement of bending capabilities of each individual section.

The applications of a large scale concentric tube robot were demonstrated through two experiments. Experiment 1 covered the capability of the robot tip to access a series of desired points in a congested space and carry out a cleaning task in a simulated hazardous environment. It was observed that the robot could access the required points in the given space within its working envelope with minimal loss of accuracy. Experiment 2 demonstrated the ability of the robot to reach through complex tight spaces and effectively use the three sections in combination to perform a remote inspection task. The proximal and middle sections provided the support and direction to the distal section for operating through the given environment.

As can be seen through the results of the experiments above, the target application for this robot is in fields where remote inspection and access is required in hazardous environments where a traditional rigid link robot or a thin long continuum robot would be

ineffective. The type of robot design introduced and evaluated in this thesis could potentially be used to perform tasks in gloveboxes used for nuclear experiments where radiation is a threatening factor and high level of dexterity is weighted over high levels of accuracy.

5.2 Suggestions for future work

The results from the tests and experiments suggest various directions in which the capabilities of the robot can be improved. The load capacity of the robot can be improved by various approaches. One could be to reduce the number of ball bearings on the distal section from 4 per spacer to 3 per spacer. Potentially, aluminum ball bearings could also be used instead of steel ball bearings. This would reduce the weight of the distal section itself and be able to improve its load capacity. Another approach could be to use a stiffer material which would provide a higher load capacity but could lower the compliance of the robot.

It was observed that reducing friction between sections was a challenge, as were torsional issues with their respective sections. These issues lower the accuracy of the robot and require to be overcome or measured in order to build a mathematical model to predict and control the movements of the robot through a simulation or an automated controller.

Currently, the mechanism allows the distal section to extend only when the middle section has extended and similarly allows the middle section to retract only when the distal section is simultaneously retracting. This can be overcome by changing the design of the linear actuation mechanism for the distal section and having a linear actuator mounted on

the 3D printed collar. This would enable the sections to actuate independently and could improve the overall capabilities of the robot.

The entire assembly could also be mounted on a motorized vehicle with a z-axis platform which could raise and lower the sections to a desired height and enable the robot to be mobile. The current assembly has the robot mounted at a fixed height which limits the reach of the robot. Having a platform capable of changing the height of the robot could help increase the working envelope of the robot.

APPENDIX

Arduino Code for Controlling TREE Using Switches

```
//Variables for DIR pins on Motor Drivers
int dr1 = 2, dr2 = 3, dr3 = 14, dr4 = 15, dr5 = 16, dr6 = 17, dr7 = 18, dr8 = 19, dr9 = 20,
dr10 = 21;
//Variables for PWM pins on Motor Drivers
int pwm1 = 4, pwm2  = 5, pwm3 = 6, pwm4 = 7, pwm5 = 8, pwm6 = 9, pwm7 = 10,
pwm8 = 11, pwm9 = 12, pwm10 = 13; //PWM1 connects to pin 7
//Variables for switches for controlling motors
int sw11 = 22, sw12 = 23, sw21 = 24 , sw22 = 25, sw31 = 26, sw32 = 27, sw41 = 28,
sw42 = 29, sw51 = 30, sw52 = 31, sw61 = 32, sw62 = 33, sw71 = 34, sw72 = 35, sw81 =
36, sw82 = 37, sw91 = 38, sw92 = 39, sw101 = 40, sw102 = 41;
//Setting a common PWM value to limit speed of motors
int pwm_val = 150;
//Setting a lower PWM value for the rotational motion motors
int pwm_rot = 90;
void setup()
{
  Serial.begin(9600);
  //Setting pinModes for all pins
  pinMode(dr1, OUTPUT);
  pinMode(pwm1, OUTPUT);
  pinMode(dr2, OUTPUT);
  pinMode(pwm2, OUTPUT);
  pinMode(dr3, OUTPUT);
  pinMode(pwm3, OUTPUT);
  pinMode(dr4, OUTPUT);
  pinMode(pwm4, OUTPUT);
  pinMode(dr5, OUTPUT);
  pinMode(pwm5, OUTPUT);
  pinMode(dr6, OUTPUT);
  pinMode(pwm6, OUTPUT);
  pinMode(dr7, OUTPUT);
  pinMode(pwm7, OUTPUT);
  pinMode(dr8, OUTPUT);
  pinMode(pwm8, OUTPUT);
  pinMode(dr9, OUTPUT);
  pinMode(pwm9, OUTPUT);
  pinMode(dr10, OUTPUT);
  pinMode(pwm10, OUTPUT);
  pinMode(sw11, INPUT);
  pinMode(sw12, INPUT);
  pinMode(sw21, INPUT);
```

```
  pinMode(sw22, INPUT);
  pinMode(sw31, INPUT);
  pinMode(sw32, INPUT);
  pinMode(sw41, INPUT);
  pinMode(sw42, INPUT);
  pinMode(sw51, INPUT);
  pinMode(sw52, INPUT);
  pinMode(sw61, INPUT);
  pinMode(sw62, INPUT);
  pinMode(sw71, INPUT);
  pinMode(sw72, INPUT);
  pinMode(sw81, INPUT);
  pinMode(sw82, INPUT);
  pinMode(sw91, INPUT);
  pinMode(sw92, INPUT);
  pinMode(sw101, INPUT);
  pinMode(sw102, INPUT);
  //Initializing the switch pins to HIGH
  digitalWrite(sw11, HIGH);
  digitalWrite(sw12, HIGH);
  digitalWrite(sw21, HIGH);
  digitalWrite(sw22, HIGH);
  digitalWrite(sw31, HIGH);
  digitalWrite(sw32, HIGH);
  digitalWrite(sw41, HIGH);
  digitalWrite(sw42, HIGH);
  digitalWrite(sw51, HIGH);
  digitalWrite(sw52, HIGH);
  digitalWrite(sw61, HIGH);
  digitalWrite(sw62, HIGH);
  digitalWrite(sw71, HIGH);
  digitalWrite(sw72, HIGH);
  digitalWrite(sw81, HIGH);
  digitalWrite(sw82, HIGH);
  digitalWrite(sw91, HIGH);
  digitalWrite(sw92, HIGH);
  digitalWrite(sw101, HIGH);
  digitalWrite(sw102, HIGH);
}

void fwd(int pwmPin, int pwmVal, int dirPin)
{
  analogWrite(pwmPin, pwmVal);
  digitalWrite(dirPin, LOW);
```

```
  Serial.println("fwd");
}

void bwd(int pwmPin, int pwmVal, int dirPin)
{
  analogWrite(pwmPin, pwmVal);
  digitalWrite(dirPin, HIGH);
  Serial.println("bwd");
}
void stp(int pwmPin, int dirPin)
{
  analogWrite(pwmPin, LOW);
  digitalWrite(dirPin, HIGH);
}

void loop()
{
  //switch 1
  if (digitalRead(sw11) == LOW)
  {
    fwd(pwm1, pwm_val, dr1);
    Serial.println("sw 11");
    digitalWrite(sw11, HIGH);
  }
  else if (digitalRead(sw12) == LOW)
  {
    Serial.println("sw 12");
    bwd(pwm1, pwm_val, dr1);
    digitalWrite(sw12, HIGH);
  }
  else
    stp(pwm1, dr1);

  //switch 2
  if (digitalRead(sw21) == LOW)
  {
    fwd(pwm2, pwm_val, dr2);
    Serial.println("sw 21");
    digitalWrite(sw21, HIGH);
  }
  else if (digitalRead(sw22) == LOW)
  {
    Serial.println("sw 22");
    bwd(pwm2, pwm_val, dr2);
```

```
  digitalWrite(sw22, HIGH);
}
else
  stp(pwm2, dr2);

//switch 3
if (digitalRead(sw31) == LOW)
{
  fwd(pwm3, pwm_val, dr3);
  Serial.println("sw 31");
  digitalWrite(sw31, HIGH);
}
else if (digitalRead(sw32) == LOW)
{
  Serial.println("sw 32");
  bwd(pwm3, pwm_val, dr3);
  digitalWrite(sw32, HIGH);
}
else
  stp(pwm3, dr3);

//switch 4
if (digitalRead(sw41) == LOW)
{
  fwd(pwm4, pwm_val, dr4);
  Serial.println("sw 41");
  digitalWrite(sw41, HIGH);
}
else if (digitalRead(sw42) == LOW)
{
  Serial.println("sw 42");
  bwd(pwm4, pwm_val, dr4);
  digitalWrite(sw42, HIGH);
}
else
  stp(pwm4, dr4);
//switch 5
if (digitalRead(sw51) == LOW)
{
  fwd(pwm5, pwm_val, dr5);
  Serial.println("sw 51");
  digitalWrite(sw51, HIGH);
}
else if (digitalRead(sw52) == LOW)
```

```
{
  Serial.println("sw 52");
  bwd(pwm5, pwm_val, dr5);
  digitalWrite(sw52, HIGH);
}
else
  stp(pwm5, dr5);

//switch 6
if (digitalRead(sw61) == LOW)
{
  fwd(pwm6, pwm_val, dr6);
  Serial.println("sw 61");
  digitalWrite(sw61, HIGH);
}
else if (digitalRead(sw62) == LOW)
{
  Serial.println("sw 62");
  bwd(pwm6, pwm_val, dr6);
  digitalWrite(sw62, HIGH);
}
else
  stp(pwm6, dr6);


//switch 7
if (digitalRead(sw71) == LOW)
{
  fwd(pwm7, 255, dr7);
  Serial.println("sw 71");
  digitalWrite(sw71, HIGH);
}
else if (digitalRead(sw72) == LOW)
{
  Serial.println("sw 72");
  bwd(pwm7, 255, dr7);
  digitalWrite(sw72, HIGH);
}
else
  stp(pwm7, dr7);

//switch 8
if (digitalRead(sw81) == LOW)
{
```

```
  fwd(pwm8, 255, dr8);
  Serial.println("sw 81");
  digitalWrite(sw81, HIGH);
 }
 else if (digitalRead(sw82) == LOW)
 {
  Serial.println("sw 82");
  bwd(pwm8, 255, dr8);
  digitalWrite(sw82, HIGH);
 }
 else
  stp(pwm8, dr8);
 //switch 9
 if (digitalRead(sw91) == LOW)
 {
  fwd(pwm9, pwm_rot, dr9);
  Serial.println("sw 91");
  digitalWrite(sw91, HIGH);
 }
 else if (digitalRead(sw92) == LOW)
 {
  Serial.println("sw 92");
  bwd(pwm9, pwm_rot, dr9);
  digitalWrite(sw92, HIGH);
 }
 else
  stp(pwm9, dr9);

 //switch 10
 if (digitalRead(sw101) == LOW)
 {
  fwd(pwm10, pwm_rot, dr10);
  Serial.println("sw 101");
  digitalWrite(sw101, HIGH);
 }
 else if (digitalRead(sw102) == LOW)
 {
  Serial.println("sw 102");
  bwd(pwm10, pwm_rot, dr10);
  digitalWrite(sw102, HIGH);
 }
 else
  stp(pwm10, dr10);
}
```

REFERENCES

[1] S. Hirose, "Biologically Inspired Robots," *Oxford University Press,* 1993.

[2] J. Burgner-Kahrs, D. C. Rucker and H. Choset, "Continuum Robots for Medical Applications," *IEEE Transactions on Robotics,* vol. 31, no. 6, pp. 1261-1280, December 2015.

[3] G. J. Bao, X. L. Ma, X. Y. Luo, T. F. Shao, L. B. Zhang and Q. H. Yang, "Full Compliant Continuum Robotic Finger and its Kinematic Model," *IJST, Transactions of Mechanical Engineering,* vol. 38, no. M2, pp. 389-402.

[4] R. V. Bostelman, J. S. Albus and R. E. Graham, "Robocrane and EMMA applied to Waste Storage Tank Remediation," in *American Nucelar Society Seventh Topical Meeting on Robotics and Remote Systems,*, Augusta, Georgia, April 1997.

[5] D. Trivedi, C. D. Rahn, W. M. Kier and I. D. Walker, "Soft Robotics: Biological inspiration, state of the art, and future research," *Applied Bionics and Biomechanics,* vol. 5, no. 3, pp. 99-111, September 2008.

[6] M. W. Hannan and I. D. Walker, "Kinematics and the implementation of an elephant's trunk manipulator and other continuum style robots," *Journal of Robotic Systems,* vol. 20, no. 2, pp. 45-63, 2003.

[7] R. J. Webster and B. A. Jones, "Design and kinematic modeling of constant curvature continuum Robots: A review," *Int. J. Robot. Res.,* vol. 29, no. 13, pp. 1661-1683, June 2010.

[8] W. McMahan, M. Pritts, V. Chitrakaran, D. Dienno, M. Grisson, B. Jones, M. Csencsits, C. D. Rahn, D. Dawson and I. D. Walker, "Field Trials and Testing of "OCTARM" Continuum Robots," *Proceedings IEEE International Conference on Robotics and Automation,* pp. 2336-2341, 2006.

[9] J. S. Mehling, M. A. Diftler, M. Chu and M. Valvo, "A Minimally Invasive Tendril Robot for In-Space Inspection," *Proceedings BioRobotics 2006 Conference,* pp. 690-695, 2006.

[10] R. Buckingham, "Snake Arm Robots," *Industrial Robot: An International Journal,* vol. 29, no. 3, pp. 242-245, 2002.

[11] M. B. Wooten and I. D. Walker, "A Novel Vine-Like Robot for In-Orbit Inspection," in *45th International Conference on Environmental Systems,* Bellevue, WA, 2015.

[12] I. D. Walker, D. Nahar, S. Verma, M. B. Wooten and A. D. Kapadia, "Challenges in Creating Long Continuum Robots," in *Proc. 21st IEEE International Conference on Methods and Models in Automation and Robotics,* Miedzyzdroje, Poland, August 2016.

[13] D. Systemes, "SOLIDWORKS," www.solidworks.com.

[14] "Cura LulzBot Edition," https://www.lulzbot.com/cura.

[15] A. Degani, H. Choset, A. Wolf and M. A. Zenati, "Highly articulated robotic probe for minimally invasive surgery," in *IEEE International Conference on Robotics and Automation*, Orlando, Florida, June 2006.

[16] S. Verma, *Accessing Corners of a Glove-box Cell using a Large-Scale Continuum Trunk Robot,* https://youtu.be/bTRitoaOBMw.

[17] S. Verma, A. D. Kapadia and I. D. Walker, *A Large-Scale Hybrid Continuum Trunk Robot,* https://youtu.be/1KdwIBba5B8.

[18] S. Verma, A. D. Kapadia and I. D. Walker, "A Large-Scale Hybrid Continuum Trunk Robot," submitted to *IEEE/RSJ International Conference on Intelligent Robots and Systems*, Vancouver, BC, Canada, September 2017.